
Article:
Hamlet Chu, H, Wei-Chan, S, Gosling, JP et al. (2016) Continuous Effector CD8+ T Cell Production in a Controlled Persistent Infection Is Sustained by a Proliferative Intermediate Population. Immunity, 45 (1). pp. 159-171. ISSN: 1074-7613

https://doi.org/10.1016/j.immuni.2016.06.013

Continuous effector T cell production by an amplifying intermediate in a controlled persistent infection

H. Hamlet Chu[1,5], Shiao-Wei Chan[1], John Paul Gosling[2], Nicolas Blanchard[3], Alexandra Tsitsiklis[1], Grant Lythe[4], Nilabh Shastri[1], Carmen Molina-París[4], and Ellen A. Robey[1,5]

[1]Division of Immunology and Pathogenesis, Department of Molecular and Cell Biology, University of California Berkeley, Berkeley, CA 94720, USA.

[2]Departments of Statistics, and [4]Applied Mathematics, School of Mathematics, University of Leeds, Leeds, UK.

[3]Center of Pathophysiology of Toulouse-Purpan, INSERM UMR1043-CNRS UMR5282, University of Toulouse, 31024 Toulouse Cedex 3, France.

[5]Correspondence to: hamletchu.berkeley@gmail.com (H.H.C.) or erobey@berkeley.edu (E.A.R.)

SUMMARY

Polyfunctional CD8+ effector T cells (T_{eff}) can persist in large quantities in mice and humans with controlled, persistent intracellular infections; however, the cellular mechanisms that maintain ongoing effector responses are unclear. Here we describe a mouse model in which an immunodominant CD8+ T cell response exerts tight control over a persistent intracellular parasitic infection: a scenario that is reminiscent of anti-HIV T cell responses in rare individuals who control the infection. We show that the continuous production of large numbers of short-lived T_{eff} cells is maintained via a proliferative, antigen-sensitive intermediate population (T_{int}) with a memory/effector hybrid phenotype. Our data highlight the importance of a T_{int} amplifying population to optimize memory/effector homeostasis during persistent infection. Targeting the T_{int} subset may serve as effective strategy for better T cell vaccines against chronic infections.

INTRODUCTION

CD8+ T cells provide protection against intracellular pathogens through a division of labor involving antigen-experienced effector and memory T cells. This process has been extensively examined in models of acute infection, in which pathogen-specific naïve CD8+ T cells rapidly expand and differentiate in response to signals from antigen and other environmental cues (Arens and Schoenberger, 2010; Jameson and Masopust, 2009; Rohr et al., 2014). Upon pathogen clearance, short-lived effector T cells (T_{eff}) die from apoptosis and a long-lived population of memory T cells (T_{mem}) remains (Joshi et al., 2007; Zehn et al., 2009). Long-lasting memory following acute infection is mediated by a stem cell-like population within the T_{mem} compartment that can self-renew or differentiate to generate new T_{eff} upon secondary challenge (Gattinoni et al., 2011; Graef et al., 2014; Luckey et al., 2006).

While the generation of T_{mem} cells has been a major focus of vaccine strategies, emerging evidence highlights the important protective function of an on-going CD8+ T_{eff} response (Masopust and Picker, 2012). For example, strong immune protection induced by a heterologous prime and boost strategy is due to a persistent T_{eff} response (Jabbari and Harty, 2006; Masopust et al., 2006; Olson et al., 2013). Likewise, a prolonged T_{eff} response is associated with protection in a promising cytomegalovirus (CMV) vector-based vaccine for simian immunodeficiency virus (SIV) (Hansen et al., 2011; Hansen et al., 2009; Watkins et al., 2008). These long-lasting T_{eff} are generally maintained by ongoing exposure to antigen (Mackay et al., 2012; Nelson et al., 2013), however in many

settings, persistent antigen leads to T cell exhaustion. Indeed, much of our knowledge regarding T cell responses to persistent infections comes from models in which pathogen control is incomplete and T cells become functionally impaired over time (Virgin et al., 2009; Wherry, 2011). Therefore, the cellular mechanisms that maintain long-lasting effective control of persistent pathogens are not well understood.

Mouse cytomegalovirus (MCMV) infection is an important experimental model for understanding ongoing CD8+ T_{eff} responses. Studies of MCMV infection in mice revealed continuous generation of T_{eff} cells from an antigen-experienced progenitor population with a memory-like phenotype (Snyder et al., 2008) and a requirement for ongoing antigen presentation to maintain the CD8+ effector response (Snyder et al., 2011; Torti et al., 2011). One complicating feature of the MCMV infection model is the late expansion of certain CD8+ T cell specificities, a phenomenon termed “memory inflation” (Karrer et al., 2003). An additional complexity is the dominant protective role of NK cells in the C57BL/6 (B6) strain of mice (Vidal and Lanier, 2006). As a result, this model has not allowed for dissection of the developmental pathway that leads to continuous CD8+ effector generation *in vivo*. Hence, there is a pressing need for new mouse infection models to investigate the mechanism of CD8+ effector maintenance during controlled persistent infection.

A key to maintaining effective CD8+ T cell control of persistent intracellular pathogens is the allelic form of the host major histocompatibility complex (MHC) locus. For example, the ability to generate highly effective T cell responses to

human immunodeficiency virus (HIV) is strongly linked to MHC-class I (MHC-I) polymorphisms that affect peptide binding (International et al., 2010; Kosmrlj et al., 2010). Moreover, HIV “elite controllers”, individuals who remain disease free without anti-viral therapy, often harbor polyfunctional CD8+ T cells specific for viral peptides presented by protective allelic forms of MHC-I (Almeida et al., 2007; Horton et al., 2006). Thus, an ideal experimental model for effective control of persistent infection may rely on particular combinations of host MHC-I and pathogen-derived antigenic peptides that can elicit unusually long lasting CD8+ T cell responses, along with a pathogen that has evolved to persist in the face of immune control.

We considered that infection of a resistant mouse strain by the intracellular protozoan parasite, *Toxoplasma gondii*, might provide such an ideal experimental model. *Toxoplasma* parasites can induce a strong CD8+ T cell response, typically establish life-long persistence in their mammalian hosts, and often produce asymptomatic infections. Moreover, mice harboring the MHC-I molecule L^d exhibit particularly effective control of the parasite, due to an immunodominant CD8+ T cell response directed against the parasite protein, GRA6 (Blanchard et al., 2008; Brown et al., 1995). In contrast, infected mice without the protective L^d MHC-I molecule develop a chronic progressive infection associated with dysfunctional T cell responses (Bhadra et al., 2011). Interestingly, both mouse MHC-I L^d, and certain human MHC-I alleles associated with elite HIV control, share key polymorphic amino acids in the peptide binding site, and exhibit limited peptide binding capacity (Kosmrlj et al., 2010; Narayanan

and Kranz, 2013). Thus, parasite infection in resistant mice shares a number of features of HIV elite control, including an atypical MHC-I allele that confers strong protection, a robust ongoing CD8+ T_{eff} response, and persistent but asymptomatic infection.

In the current study, we examine the anti-*T. gondii* CD8+ T cell response in genetically resistant mice to gain insight into the maintenance of highly effective T cell responses. We show that low-level persisting antigen presentation drives continuous production of polyfunctional T_{eff} without a notable contraction phase. Using a combination of the effector marker KLRG1, and the chemokine receptor CXCR3, we identify three subsets of antigen-experienced CD8+ T cells whose numbers are maintained over time by balanced proliferation, differentiation, and cell death. In addition to a relatively quiescent, memory like population, and a terminally differentiated T_{eff} population, we also identify a metabolically active intermediate population, which has a hybrid memory/effector phenotype, and is strongly dependent on persistent antigen for its survival, proliferation and T_{eff} differentiation. Our results reveal that highly effective CD8 T cell control of a persistent pathogen is maintained by a division of labor in which a T_{int} subset allows for efficient and flexible generation of T_{eff} in response to changing antigen levels, while a T_{mem} population provides for long-term maintenance of the response.

RESULTS

The CD8+ T cell response to *T. gondii* in genetically resistant mice exhibits immunodominance, and a long-lasting polyfunctional effector response.

Strong immune protection against the persistent intracellular protozoan parasite *Toxoplasma gondii* in genetically resistant mice is linked to the MHC-I allele L^d and presentation of a single antigenic peptide derived from the parasite dense granule protein, GRA6 (Blanchard et al., 2008). We compared the anti-GRA6:L^d response to subdominant CD8+ GRA4:L^d- and ROP5:D^b-specific T cell responses (Frickel et al., 2008; Grover et al., 2014) using F1 (H-2^{bxd}) mice orally infected with tissue cysts generated from the type II *T. gondii* strain, *Prugniaud* (Pru). The number of infected cells in both the draining mesenteric lymph nodes (MLN) and spleen peaked at 7 days after infection and then declined to undetectable levels by day 21. We detected a low but persistent level of *T. gondii* DNA in the brain beginning 11 days after oral infection (Figure 1A), reflecting the ability of *T. gondii* to establish chronic infection by encysting in the brain (Ferguson et al., 1989). In spite of parasite persistence, infected hosts did not show any sign of illness at >6 months post infection (data not shown), confirming the resistance of mice expressing the L^d allele of MHC-I (Brown et al., 1995).

To compare multiple CD8+ T cell populations in the same animal, we used fluorochrome-labeled peptide-MHC-I (pMHC-I) tetramers to detect *T. gondii*-specific T cells *ex vivo* by flow cytometry. At day 21 after infection, GRA6:L^d-specific CD8+ T cells represented ~20% of total CD8+ T cells, and were 100-fold more abundant than the subdominant GRA4:L^d- and ROP5:D^b-specific T cells (Figure 1B). At day 11, the subdominant T cells expanded only 40-200 fold

relative to their numbers at day 3, whereas splenic GRA6:L^d-specific T cells expanded ~10,000 fold to ~$5x10^5$ cells/spleen during the same time period, and continued to expand to reach the peak of ~10^6 cells/spleen at 21 days post infection (Figure 1C). Anti-GRA6:L^d-specific T cells peaked at day 21 in the brain and persisted to at least day 200 after infection, while the subdominant T cells were 100-fold less numerous (Figure 1C). The majority of brain GRA6:L^d-specific T cells were not labeled by intravenous injection of CD45.1 antibody, indicating they resided in the brain parenchyma, and exhibited a phenotype consistent with tissue-resident memory T cells (Figure S1A and S1B) (Wakim et al., 2010). Intriguingly, the number of *T. gondii*-specific T cells in the spleen was maintained near peak levels throughout the chronic phase of infection in spite of the sharp decline in parasite load (Figure 1A and 1C). Hence, the *T. gondii*-specific CD8+ T cell response in resistant mice is characterized by rapid expansion of a single T cell specificity, and maintenance of large parasite-specific T cell population without a contraction phase.

While the loss of T cell effector function, termed T cell exhaustion, is observed in many chronic infections (Virgin et al., 2009), GRA6:L^d-specific T cells from chronically infected mice exhibited potent *in vivo* killing activity and produced high levels of IFNγ and TNFα simultaneously upon brief *ex vivo* restimulation (Figure 1D and 1E). T cells specific for subdominant parasite antigens, in addition to their reduced numbers, produced lower levels of IFNγ and the majority failed to co-express TNFα (Figure 1E). GRA6:L^d-specific T cells also maintained higher expression of the effector marker KLRG1, and lower

expression of the memory marker CD62L compared to the subdominant T cell responses (Figure 1F). *T. gondii*-specific T cells also lacked expression of the T cell exhaustion marker PD-1 during the chronic phase of infection, expressing it only transiently during the expansion phase (Figure 1F). Thus, the CD8+ GRA6:L^d-specific T cell response is characterized by a large, polyfunctional effector population that persists throughout chronic infection.

Persistent antigen presentation correlates with GRA6:L^d-specific T cell proliferation during the chronic phase of infection.

The lack of a contraction phase and persistent effector function suggested that a low level of antigen presentation during the chronic phase of infection might drive the continuous generation of new T_{eff} cells. To measure antigen presentation *in vivo*, we transferred naïve GRA6:L^d-specific transgenic T cells (TG6) (Figure S2) into previously infected mice and assessed their proliferation 3 days after transfer (Figure 2A). Substantial proliferation was observed when naïve TG6 T cells were transferred into mice that had been infected 140 days earlier with Pru strain parasites, but not in mice infected with a parasite strain that lacks the GRA6 epitope (Figure 2B). Thus, in spite of parasite clearance from secondary lymphoid organs (Figure 1A), GRA6 antigen presentation persisted late into chronic infection.

We also observed that 5-10% of total GRA6:L^d-specific cells in chronically infected mice were in cell cycle, based on expression of the proliferation marker Ki67, and overnight *in vivo* incorporation of the DNA analog EdU (Figure 2C and

2D). Interestingly, the decline of antigen presentation after initial infection correlated with the gradual reduction in the proportion of GRA6:L^d-specific T cells in cycle (Figure 2C). Together, these data suggest that persistent GRA6 antigen presentation drives the proliferation of a subset of GRA6:L^d-specific T cells during chronic infection.

GRA6:L^d-specific T cell immunodominance correlates with the predominance and persistence of a CXCR3+KLRG1+ population.

Ongoing proliferation within the numerically stable GRA6:L^d-specific T cell population implies that the population size is maintained dynamically by continuous production of new cells balanced by cell loss. To investigate these population dynamics, we examined the composition of the dividing and non-dividing GRA6:L^d-specific T cell populations in more detail.

The GRA6:L^d-specific T cell response did not appear to be maintained by precursor population with a classic central memory phenotype (Sallusto et al., 1999), since antigen experienced GRA6:L^d specific T cells were uniformly CCR7-CD62L- (Figure S3A). In addition, while the combination of markers often used to distinguish effectors from memory precursors (KLRG1 and CD127)(Joshi et al., 2007) divided the population into three subsets, the proliferating population was equally distributed between these subsets (Figure S3B and S3C). In contrast, the combination of KLRG1 and CXCR3 revealed a KLRG1+CXCR3+ population that was highly enriched for proliferating cells (Figure S3B and S3C).

We also noted that the antigen experienced T cell subsets defined by CXCR3 and KLRG1 differ in their proportions between dominant GRA6 and subdominant GRA4/ROP5 specificities (Figure 3A). In particular, the GRA6:L^d-specific T cells consistently contained a higher proportion of CXCR3+KLRG1+ cells compared to the GRA4:L^d/ROP5:D^b-specific T cells (Figure 3A and 3B). Moreover, the CXCR3+KLRG1+ subset of the GRA6:L^d-specific population persisted throughout infection, whereas the CXCR3+KLRG1+ subset in the GRA4:L^d/ROP5:D^b-specific T cells exhibited a marked decline between days 10-42 of infection and became barely detectable by day 60 after infection (Figure 3A and 3B). Thus, GRA6:L^d-specific T cell immunodominance correlates with the predominance and stability of the CXCR3+KLRG1+ population.

Recent thymic emigrants (RTEs) were reported to contribute to the stability of the antigen-specific CD8+ T responses in some persistent infections (Snyder et al., 2008; Vezys et al., 2006). To examine the role of RTEs in maintaining the GRA6-specific T cell population, we transferred a small number of naïve TG6 T cells into congenic recipients before oral infection, and enumerated TG6 cells over the course of infection. All three CXCR3/KLRG1 subsets in donor TG6 T cells demonstrated similar kinetics to the endogenous GRA6:L^d-specific T cells, highlighted by maintenance of the near-peak numbers and the lack of contraction (Figure 3C). These data indicate that a stable GRA6-L^d-specific T cell population can be maintained over time without contribution from recent thymic emigrants.

The CXCR3+KLRG1+ subset has both memory and effector cell characteristics

To better understand the relationship of the CXCR3/KLRG1 populations to previously defined memory and effector T cells, we performed additional flow cytometric analysis of GRA6:L^d-specific CD8+ T cells from chronically infected mice. As expected based on Ki67 staining (Figure 4A, Figure S2B and S2C), CXCR3+KLRG1+ cells incorporated the highest level of the thymidine analog EdU after an overnight labeling (Figure 4A), confirming that most proliferating cells are found within this subset. CXCR3+KLRG1+ cells also had the highest levels of the nutrient update receptors, CD71 and CD98 (Figure 4A) implying that they are more metabolically active. CXCR3+KLRG1+ subset expressed relatively low levels of the anti-apoptotic molecule Bcl-2 (Figure 4B) and high levels of the effector marker Blimp-1, but also expressed a memory associated phenotype of CD122+, $CD27^{hi}CD43^{lo}$ (Hikono et al., 2007), and $Eomes^{hi}$ (Banerjee et al., 2010) (Figure 4C). *In vitro* cytotoxicity assays on sorted CXCR3/KLRG1 populations (Figure S3D to S3E) demonstrated that the CXCR3-KLRG1+ subset harbored the strongest cytotoxicity, followed by the CXCR3+KLRG1+ subset, while the CXCR3+KLRG1- subset exhibited minimal killing capacity (Figure S3F). Thus, the CXCR3/KLRG1 gating strategy subdivided anti-*T. gondii* CD8+ T cells into three subsets of distinct functions and phenotypes, and identified a proliferative CXCR3+KLRG1+ subset with both memory and effector cell characteristics.

Lineage relationship and antigen dependence of the CXCR3/KLRG1 subsets.

To explore the developmental relationship among the CXCR3/KLRG1 subsets, we sorted GRA6:L^d-specific CXCR3/KLRG1 subsets from infected mice and followed their fates upon transfer into congenically marked infected recipients (Figure S4A). GRA6:L^d-specific CXCR3+KLRG1- and CXCR3+KLRG1+ cells proliferated and expanded 35 and 19 fold respectively between days 2 and 21 after transfer, whereas majority of the CXCR3-KLRG1+ cells did not proliferate, and their numbers declined with a half-life of 28 days (Figure 5A and 5B). Interestingly, CXCR3+KLRG1- cells gave rise to all three subsets after transfer, whereas CXCR3+KLRG1+ cells gave rise only to CXCR3+KLRG1+ and CXCR3-KLRG1+ cells, and finally, CXCR3-KLRG1+ cells maintained their phenotype (Figure 5B). Similar CXCR3/KLRG1 profiles were obtained upon transfer of CXCR3/KLRG1 subsets into T and B cell deficient (*rag*$^{-/-}$) mice during acute infection, although both donor CXCR3+ subsets underwent greater expansion compared to transfer into wild type recipients (Figure S4B). In summary, these experiments support the lineage relationship of CXCR3+KLRG1- ➔ CXCR3+KLRG1+ ➔ CXCR3-KLRG1+, and confirm that CXCR3-KLRG1+ cells are terminally differentiated.

To examine the role of antigen in the differentiation and survival of the CXCR3/KLRG1 subsets, we transferred sorted populations into naïve recipients. Twenty-one days after transfer all donor CXCR3/KLRG1 subsets maintained their phenotypes, and the majority had not divided (Figure 5C). Based on the

recovery of donor cells at day 2 and day 21 post transfer, CXCR3+KLRG1- cells showed the greatest survival with a half-live of 89 days, whereas CXCR3+KLRG1+ and CXCR3-KLRG1+ subsets displayed half-lives of 10 and 20 days respectively (Figure 5D). These relative half-lives are consistent with the expression of anti-apoptotic protein Bcl-2, which is lowest in the short-lived CXCR3+KLRG1+ population (Figure 4B). These data suggest that antigen is required for differentiation and proliferation of both CXCR3 expressing subsets. Based on their developmental order, phenotype and functional properties, we hereafter refer to CXCR3+KLRG1- cells as T_{mem}, CXCR+KLRG1+ cells as T_{int}, and CXCR3-KLRG1+ cells as T_{eff}.

Persistent antigen presentation prevents T cell contraction by sustaining the amplifying T_{int} population.

The results from cell transfer experiments and the strong antigen-dependence of the T_{int} population imply that maintenance of this population by residual antigen is key to preventing T cell contraction following activation and expansion. To further test this idea, we examined the GRA6:L^d specific response to irradiated parasites, which can invade host cells and trigger a CD8+ T cell response, but fail to establish chronic infection *in vivo* (Hiramoto et al., 2002). To allow for a similar infection in the acute phase, we used an intraperitoneal (i.p.) route of infection with either 10^6 irradiated parasites or 10^5 live parasites. Initial levels of GRA6 antigen presentation and early T cell expansion were comparable after injection of either irradiated or live parasites (Figure 6A and 6B). However,

while antigen levels remained high 42 days after infection of mice with live parasites, antigen levels in mice injected with irradiated parasites were markedly reduced by day 12 and undetectable at day 42 post-infection (Figure 6A). Transient antigen presentation in mice infected with irradiated parasites correlated with a 80% loss of total GRA6:L^d-specific T cells between day 12 and day 21 (Figure 6B) and a sharp reduction in the proportion of Ki67+ cells (Figure 6C). In contrast, mice infected i.p. with live parasites exhibited little or no contraction phase (Figure 6b), and ongoing proliferation within T_{mem} and T_{int} subsets (Figure 6C), similar to the results obtained from orally infected mice (Figure 3). Interestingly, while all CXCR3/KLRG1 subsets declined during the contraction phase, the greatest reduction in cell number occurred in the T_{int} subset (Figure 6D and 6E). These data are consistent with the relative half-lives of the 3 populations following transfer into naïve mice (Figure 5D), and confirm that the T_{int} subset is particularly dependent on persistent antigen for its survival and proliferation.

We considered that a decline in presentation of the subdominant antigens could help to explain the loss of the T_{int} population amongst T cells responding to these antigens (Figure 3A and 3B). To test this idea, we examined the *in vivo* kinetics of presentation of the subdominant antigen ROP5, by transferring naïve T cells from ROP5:D^b-specific TCR transgenic mice (termed TR5 mice, Figure S5) into infected mice. Unlike the gradual reduction observed for the GRA6 antigen (Figure 6F and Figure 2C), presentation of the ROP5 antigen dropped sharply between days 13 to 50, corresponding to the kinetics of loss of the

tetramer+ T_{int} T cells (Figure 6F). These data further support the importance of persistent antigen and the T_{int} population in maintaining an ongoing T cell response, and also help to explain the immunodominance of the GRA6:L^d-specific T cell population.

Mathematical modeling illustrates the role of the amplifying T_{int} subset in sustaining a robust T_{eff} response.

The ability of the T_{mem}, but not the T_{int} population, to replenish all 3 subsets and survive in the absence of antigen implies that the T_{mem} population supports the long-term maintenance of the GRA6:L^d-specific effector response, while T_{int} cells provide short-term amplification of the response. Consistent with this notion, T_{int} in chronically infected mice exhibit a relatively high proliferation rate, whereas T_{mem} are relatively quiescent (Figure 4A).

To further explore the roles of T_{mem} and T_{int} subsets in maintaining the T_{eff} response, we considered two alternative models. In one model, T_{mem} can divide to either produce another T_{mem} cell (self-renewal) or differentiate directly into a non-dividing T_{eff} cell (Figure 7A). A second model includes a T_{int} population that can divide to produce another T_{int} cell (amplification) or can differentiate into a non-dividing T_{eff} (Figure 7B and Figure 5A, see also Experimental Procedures). In both models, we assumed that T_{eff} disappear with a constant death rate of 0.027 cells/day (i.e. 2.7% of total T_{eff} die each day) based on the cell transfer experiments in Figure 4B.

We first used model 1 to explore the range of T_{mem} self-renewal and differentiation rates that would allow for the observed overall rate of T_{eff} production of $2.5x10^6$ T_{eff} from 10^5 T_{mem} at steady state (Figure 3B). By varying T_{mem} self-renewal and differentiation rates ($\lambda 1$ and $\xi 1$, respectively), we found that the self-renewal rate $\lambda 1$ had to be greater than 0.3 cells/day to generate $2.5x10^6$ T_{eff} at steady state (Figure 7C). This value is incompatible with the observed low rate of proliferation within the T_{mem} population (i.e. 6% of the T_{mem} population was labeled with EdU in every 14 hours, or 0.1 cells/day, see also Figure 4A). Moreover, increasing the differentiation rate to approach the self-renewal rate led to a sharp decline in the number of effectors, due to the depletion of the T_{mem} population (Figure 7C and data not shown).

To evaluate the plausibility of model 2, we varied the T_{int} amplification and differentiation rates ($\lambda 2$ and $\xi 2$, respectively) while leaving the remaining parameters set at control values estimated from available experimental data (Table S1A, see also Experimental Procedures), and calculated the number of T_{eff} at steady state (Figure 7D). We observed that an amplification rate ($\lambda 2$) of 0.5 cells/day or greater would allow for the generation of $2.5x10^6$ T_{eff} at steady state (Figure 7D). This value is in line with observed rate of proliferation within the T_{int} population (i.e. 29% EdU-labeled cells in 14 hours, or 0.5 cells/day, see also Figure 4A). Moreover, unlike model 1, in which increasing the differentiation rate led to a precipitous drop in T_{eff} production (Figure 7C), increasing the differentiation rate $\xi 2$ for model 2 led to a gradual decline in T_{eff} numbers and never led to complete elimination of the response (Figure 7D). We also observed

that the theoretical time course generated using model 2 and control parameters (Table S1A) correlated well with the experimental data derived from both the steady state cell number and cell transfer experiments (Figure 7E, Figure 3, and Figure 5A). These data suggest how the T_{int} population can allow for rapid high-level production of T_{eff} cells (Figure S6), and can modulate the rate of differentiation of T_{eff} without depleting a key progenitor population needed to sustain the response over the long-term.

DISCUSSION

An ongoing T cell effector response is key to protective T-cell based vaccines, as well as natural resistance to persistent intracellular pathogens such as HIV (Masopust and Picker, 2012). However, the mechanisms that maintain robust T cell effector responses are largely unknown, due in part to the lack of appropriate mouse infection models. Here we show that persistent, asymptomatic *T. gondii*-infection in genetically resistant (H-2^d) mice gives rise to a robust immunodominant CD8+ effector response that is maintained over time without a contraction phase, and without any signs of functional exhaustion. We investigated the cellular mechanisms that maintain this effector response, revealing a division of labor in which a relatively quiescent and long-lived memory population (T_{mem}) gives rise to terminally differentiated effector cells (T_{eff}) via a proliferative, antigen-sensitive intermediate population (T_{int}). Our data provide novel insight into the cellular dynamics that maintain robust ongoing CD8+ T cell effector responses, and highlight the importance of an amplifying T_{int}

population to generate adequate numbers of new T_{eff} in response to changing pathogen levels, while preserving a long-lived T_{mem} population.

Achieving a stable, asymptomatic standoff between an intracellular pathogen and an ongoing T_{eff} response requires both a pathogen that is able to occupy a long-term niche in the host, and a T cell response with appropriate specificity to provide highly effective immune control. With regard to the latter, it is intriguing to note that MHC-I variants associated with HIV elite control, and the MHC-I molecule L^d that presents the immunodominant parasite antigen GRA6, share structural features including atypical peptide binding properties (International et al., 2010; Kosmrlj et al., 2010; Narayanan and Kranz, 2013). For the GRA6 antigen, a number of other factors contribute to efficient antigen presentation, including the secretion pattern of the antigenic protein within the invaded host cell, and the location of the epitope within the precursor protein (Feliu et al., 2013; Grover et al., 2014; Lopez et al., 2015). Thus, both features of a particular antigenic protein and presentation by an atypical MHC-I molecule may contribute to generating an unusually protective CD8+ T cell response.

In addition to the protective pressure exerted by T cells, the ability of certain pathogens to adopt a relatively latent form in the host also contributes to the stable standoff between pathogen and host immune response. We showed that continued presence of the parasite, leading to persistent low-level antigen presentation, is required to prevent T cell contraction and maintain robust T_{eff} responses. *T. gondii* is able to achieve long-term persistence by converting to a relatively dormant, cyst-forming stage in the brain of its infected host (Montoya

and Liesenfeld, 2004). Likewise the ability of β-herpesvirues, including cytomegalovirus (CMV), to adopt a latent form in mammalian host cells, likely provides a continuous source of antigen, which may explain the remarkable potency and longevity of T_{eff} responses elicited by a CMV-based vaccine against SIV in non-human primates (Hansen et al., 2011; Hansen et al., 2009). Interestingly, heterologous prime-boost vaccination strategies can generate long lived effector responses without persistent infection (Jabbari and Harty, 2006; Masopust et al., 2006; Olson et al., 2013). However, there can be sustained antigen presentation after acute viral infection (Turner et al., 2007), in part due to formation of immune-complexes (Leon et al., 2014).

A large body of literature using acute infection models has subdivided antigen-experienced CD8+ T cells into effector and memory populations based on cell surface markers including CCR7, CD62L, CD127 (IL7Rα), and KLRG1 (Joshi et al., 2007; Sallusto et al., 1999; Wherry et al., 2003). Interestingly, the distinction between central memory (CCR7+CD62L+) and effector memory (CCR7-CD62L-) (Sallusto et al., 1999; Wherry et al., 2003) does not appear to be relevant in this infection model, since antigen experienced GRA6:L^d-specific CD8+ T cells were uniformly low for CCR7 and CD62L. This included the CXCR3+KLRG1- population that could give rise to all other subsets and was long-lived in the absence of antigen, and thus resembled a memory population. Moreover, CD127, which has been used in conjunction with the effector marker KLRG1 to distinguish memory precursor versus short-lived effectors (Joshi et al., 2007), does not appear to be useful marker in this infection model. Rather,

transition from CXCR3+KLRG1+ T_{int} to CXCR3-KLRG1+ T_{eff} phenotype correlated with the loss of proliferation and terminal differentiation of effector cells. Interestingly, Yap and colleagues observed cycling T cells of CXCR3+KLRG1+ phenotype in an acute *T. gondii* vaccination model, and found that T_{eff} terminal differentiation correlated with CXCR3 downregulation in an IL-12 and IFNγ dependent manner (Kohlmeier et al., 2011; Kurachi et al., 2011; Shah et al., 2015). Together with our results, these findings suggest that the precise timing of TCR and cytokine/chemokine signals may be important for regulating T cell amplification and effector differentiation during infection by modulating the CXCR3+KLRG1+ T_{int} subset.

Our modeling studies point to the role of T_{int} cells in maintaining an ongoing T_{eff} response. Without the T_{int} population, T_{mem} cells would need to proliferate extensively to keep up with the demand for new T_{eff} cell output. Moreover, if increasing antigen levels were to drive more rapid differentiation into T_{eff}, this would lead to the depletion of the T_{mem} population and eventually the collapse of the T cell response. Hence the presence of the T_{int} population allows for rapid production of new T_{eff}, while maintaining a relatively quiescent T_{mem} population when antigen levels remain constant, and provides extra capacity for increasing T_{eff} differentiation in response to increasing antigen levels.

One interesting feature of the T_{int} population is high expression of the T-box transcription factor Eomes. Eomes, and the related transcription factor T-bet play partially redundant roles in CD8+ T cells, although Eomes also plays unique roles in the maintenance of memory and exhausted T cells (Banerjee et al.,

2010; Intlekofer et al., 2005; Paley et al., 2012). Interestingly, high Eomes expression is also associated with a proliferative subset of CD8+ T cells found some HIV-infected individuals, which correlates with effective viral control (Simonetta et al., 2014). Moreover, Eomes is expressed at high levels in intermediate neural progenitor cells, where it is required for the maintenance of the intermediate population and ongoing neurogenesis (Hodge et al., 2008; Hodge et al., 2012). Understanding the precise role of Eomes in maintaining robust CD8+ T cell effector responses during persistent infection is an important area for future investigation.

In summary, we used a controlled persistent *T. gondii* infection model to delineate the cellular mechanism that sustains a long-term CD8+ T_{eff} response. We identified a novel T cell intermediate subset that provides for efficient effector cell output, and is responsive to antigen levels. Approaches to manipulate the size of the T_{int} subset, perhaps via regulated release of antigen, may improve the efficacy of current vaccine regimens by sustaining robust T_{eff} responses (Beura et al., 2014; Demento et al., 2012), while preserving a stable T_{mem} population.

EXPERIMENTAL PROCEDURES

Animals

B6 (C57BL/6), B6 Rag2$^{-/-}$ (B6-Cg-*Rag2*$^{tm1.1Cgn}$/J), B6.C (B6.C-*H2d*/bByJ), BALB/c, BALB/c Rag2$^{-/-}$ (C.B6(Cg)-*Rag2*$^{tm1.1Cgn}$/J), CBA, CD45.1+ congenic B6 (B6.SJL-*Ptprc*^{a} *Pep3*^{b}/BoyJ), B6 Blimp1-YFP reporter (B6.Cg-Tg Prdm1-EYFP 1Mnz/J) were obtained from The Jackson Laboratory (Bar Harbor, ME) or The Charles River Laboratory (Wilmington, MA). In order to monitor multiple *T. gondii* epitopes, F1 mice (B6xB6.C or B6xBALB/c) expressing both the H-2^{b} and H-2^{d} MHC class I molecules were used for all experiments. For adoptive transfer experiments, only B6xB6.C F1 mice were used. This included the GRA6:L^{d}-specific and the ROP5:D^{b}-specific TCR transgenic (TG6 and TR5, respectively) mice, which were maintained on the B6 background and were then bred with B6.C mice to F1 background (H-2$^{b/d}$). All animals were used or infected between

six to ten week-old. For all infection and adoptive transfer experiments, sex- and age-matched genetically homogeneous mice were used, therefore no randomization was required. Mice bred in UC Berkeley animal facility and were used with the approval of the Animal Care and Use Committee of the University of California.

Infection

Mice were orally fed 70-80 cysts or injected intraperitoneally (i.p.) with 1×10^5 live tachyzoites from the type II Prugniuad-tomato-OVA strain (Pru)(Chtanova et al., 2008). This strain harbors immunogenic T cell epitopes derived from the parasite proteins, GRA6 (Blanchard et al., 2008), GRA4 (Frickel et al., 2008), and ROP5 (Grover et al., 2014), and is engineered to express red fluorescent protein (RFP), allowing for tracking infected cells by flow cytometry. In some experiments, mice were immunized i.p. with $1x10^6$ irradiated Pru tachyzoites (14,000 rads). In other experiments, tachyzoites from type III CEP strain parasites were used for infection. CEP expresses an allelic version of GRA6 that lacks the T cell-stimulatory epitope (Grover et al., 2014), and is used here as a negative control. Cysts were obtained from brains of CBA mice infected for 3–5 weeks i.p. with 400 live Pru tachyzoites. Parasite loads in spleen and lymph nodes was analyzed by flow cytometry and parasite load in the brain was analyzed by semi-quantitative PCR (Grover et al., 2014).

Generation of the *T. gondii* GRA6:L^d-specific (TG6) and ROP5:D^b-specific (TR5) TCR transgenic mice

The TCR alpha and beta chain sequences of the GRA6:L^d-specific CTgEZ.4 T cell hybridoma (Blanchard et al., 2008) were determined according to Kraig et al (Kraig et al., 1996). The GRA6:L^d-specific and ROP5:D^b-specific TCRs corresponded to TRAV6-7/DV9*01, TRAJ52*01. Then, both TCR chains were cloned and amplified from the genomic DNA of the CTgEZ.4 cell line by using forward primer specific for TRAV6-7/DV9 (5'-TCTCCCGGGGTCTAAAGATGAACTCTTCTCCAGG) and reverse primer for TRAJ52 (5'-TAAGCGGCCGCTGAGCGC AGTAAAGATT CTAGC); forward primer specific for TRBV1*01 (5'-TCT CTCGAG TCTCAGAGATGTGGCAGTTTTGC) and reverse primer for TRBJ2-1 (5'-TAAG CCGCGG TCCTGGAAATGCTGGCACAAACC). Similarly, the ROP5:D^b-specific TCR alpha and beta chains were cloned and amplified from the genomic DNA of the BTg45Z cell line (Grover et al., 2014) by using forward primer specific for TRAV10 (5'- TCT CCC GGG GGA AGA ATG ATG AAG ACA TCC CTT CAC AC) and reverse primer for TRAJ49 (5'- TAA GCG GCC GCG TCT TGG TGA GTG AGC AAG ACA GAA G); forward primer specific for TRBV13-3 (5'- TCT CTC GAG TTCTGAG ATG GGC TCC AGA CTC TTC) and reverse primer for TRBJ2-5 (5'- TAAG CCG CGG CGC CCA CTG CAG CCC AAT CCC GCT GAG).

In all cases, the TCR alpha chains were then cloned into pTa cassette vector in Xmal and Not1 sites, while the TCR beta chains were cloned into pTb cassette

vector in XhoI and SacII sites, according to Kouskoff et al (Kouskoff et al., 1995). The ampicillin resistance gene was cut out with Sal I in pTa vectors and Kpn I in pTb vector before DNA injection. The TG6 transgenic mice were generated on the B6 background in the Cancer Research Laboratory Gene-Targeting Facility at UC Berkeley under standard procedures. The TR5 transgenic mice were generated on the B6 background in UC Davis Mouse Biology Program under standard procedures. Founders were identified by flow cytometry and PCR genotyping of tail genomic DNA using primers mentioned above. The TG6 and TR5 mice used in all experiments were bred with B6.C mice to generate F1 ($H\text{-}2^{bxd}$) background.

Flow cytometry

All antibodies were from eBioscience (San Diego, CA), Biolegend (San Diego, CA) or Tonbo Biosciences (San Diego, CA), except for FITC-labeled anti-mouse T-bet antibody (Santa Cruz Biotech. Inc., Santa Cruz, CA). The GRA6:L^d, GRA4:L^d, and ROP5:D^b tetramers were made by conjugating the biotin-labeled monomers (NIH tetramer facility, Atlanta, GA) with PE-labeled or APC-labeled streptavidin (Prozyme, Hayward, CA) according to protocols from the NIH tetramer facility. Brain samples were perfused and digested by collagenase before leukocytes isolation by 70%:30% percoll gradient (GE Heathcare, Pittsburgh, PA) (Grover et al., 2014). In some experiments, 3µg of FITC-labeled anti-CD45.1 (A20) antibody was injected intravenously into chronically infected mice 2 minutes before sacrifice and organ harvest (Anderson et al., 2014). In all experiments, cell suspension from the brain, lymph nodes and the spleens was incubated with tetramers and surface antibodies against mouse CD8 (53-6.7), B220 (RA3-6B2), CD27 (LG.7F9), CD44 (IM7), CD45.1 (A20), CD49d (R1-2), CD62L (MEL-14), CD122 (TM-β1), CD127 (A7R34), CXCR3 (CXCR3-173), PD-1 (RMP1-30) and/or KLRG1 (2F1) for 1 hour at 4°C. For EdU labeling experiments, previously infected mice were injected intraperitoneally with 2mg EdU (5-ethynyl-2'-deoxyuridine) for 14 hours before sacrifice. Cell suspensions were then stained with APC-labeled tetramers and other surface markers before EdU detection procedure during the Click-iT EdU Alexa-Fluor 488 Flow Cytometry Kit (Invitrogen, Carlsbad, CA) according to manufacturer's instruction. For all intracellular staining, samples stained with surface antibodies were fixed with Cytofix/Cytoperm kit (BD Pharmingen, San Diego, CA) or Transcription Factor Staining Buffer Set (eBioscience), followed by antibodies staining of intracellular TNFα (A20), IFNγ (XMG1.2), T-bet (4B10), Eomes (Dan11mag), Ki67 (SolA15) and Bcl2 (10C4). All flow cytometry data were acquired by BD LSRFortessa analyzers (BD Biosciences) and were analyzed with FlowJo software (Tree Star, Ashland, OR). Fluorescent AccuCheck counting beads (Invitrogen) were used to calculate total numbers of live lymphocytes from all samples.

***ex vivo* cytokine production assay**

Splenocytes from mice 60-140 days post infection were cultured with GRA6 peptide or GRA4 and ROP5 peptide (Peptide2.0 Inc., Chantilly, VA) in media for 4 hours with the presence of protein secretion block (eBioscience). Cells were

then harvested for surface and intracellular antibody staining before flow cytometry analysis.

GRA6 and ROP5 antigen presentation detection *in vivo*

To provide a sensitive method to detect ongoing antigen presentation, we adopted a detection method in Turner et al (Turner et al., 2007). In brief, we harvested from lymph nodes (LNs) and spleen of CD45.2+ TG6 or TR5 mice $H2^{bxd}$ background, labeled with the cell proliferation dye eFluor 450 (eBioscience, San Diego, CA), transferred cells containing 10^5 TG6 or TR5 cells into previously CD45.1+ infected mice, and examined proliferation dye dilution 3 days later as a measure of GRA6 or ROP5 antigen presentation. Relative antigen levels are expressed as the % of donor TG6 or TR5 cells that have diluted proliferation dye (proliferation dye^{low}) 3 days after transfer.

Adoptive transfer

To expand TG6 cells *in vivo*, cells were harvested from lymph nodes (LNs) and spleen of CD45.2+ TG6 mice on $H2^{bxd}$ background and transferred into CD45.1+ naïve F1 recipients at 10,000-100,000 CD8+ TG6 cells/mouse one day before infection. For FACS sorting, pooled LNs and spleen cells from multiple recipients ≥day 21 post infection were subjected to CD4+ T cell and B cell depletion by PE-labeled anti-CD4 and anti-B220 antibodies and anti-PE magnetic beads (Miltenyi Biotec. Inc., San Diego, CA) according to the manufacturer's instruction, followed by eFluor450 proliferation dye labeling. CXCR3+KLRG1-, CXCR3+KLRG1+, and CXCR3-KLRG1+ CD8+ TG6 cells were then sorted at ≥ 92% purity by a BD influx cell sorter (BD Biosciences). Each sorted subset was then transferred to naïve or >day 21 post-infected secondary recipients at 10^5 cells/mouse. Donor TG6 cells were harvested between day 2 to day 21 post transfer for flow cytometry analysis. In some experiments, sorted TG6 cells were transferred to F1 $rag^{-/-}$ mice that were infected 1 day before transfer. Donor cells were harvested 8 days after transfer for flow cytometry analysis.

***In vitro* cytotoxicity assay**

Sorted subsets of CXCR3+KLRG1-, CXCR3+KLRG1+, and CXCR3-KLRG1+ CD8+ TG6 cell subsets were obtained from infected mice as described above for adoptive transfer. Each subset was cultured with GRA6-peptide-pulsed and PBS-pulsed splenocytes from congenically marked naïve F1 mice at 1:5:5 ratio. The GRA6-peptide-pulsed and PBS-pulsed splenocytes were distinguished by different intensity of CFSE labeling (5-(and-6)-Carboxyfluorescein Diacetate, Succinimidyl Ester, Invitrogen). Cytotoxicity was assessed by the loss of the GRA6-peptide-pulsed splenocytes relative to the PBS-pulsed control after 18 hours of culture.

***In vivo* cytotoxicity assay**

Splenocytes from F1 naïve mice were labeled with cell proliferation dye eFluor 450 at four different levels of intensity. Each labeled population was then pulsed with either 1μM of GRA6, GRA4, ROP5-pepitdes (Peptide2.0 Inc.) or PBS for 1

hour at 37°C. Pulsed cells were then washed twice and mixed at 1:1:1:1 ratio with 10^6 cells from each population. Cell mixture was injected intravenously into chronically infected mice and harvested 18 hours later.

Mathematical modeling and Bayesian statistical analysis

To construct the mathematical models for Figure 7, we made the following assumptions: **1a)** Model 1 follows the linear order: T_{mem} (CXCR3+KLRG1-, called x1) ➔ T_{eff} (CXCR3-KLRG1+, called x3); **1b)** Model 2 follows the linear order: T_{mem} (CXCR3+KLRG1-, called x1) ➔ T_{int} (CXCR3+KLRG1+, called x2) ➔ T_{eff} (CXCR3-KLRG1+, called x3); **2)** T_{eff} do not proliferate or further differentiate, and eventually die (death rate, $\mu 3$). **3)** Populations x1 and x2 are characterized by an intrinsic carrying capacity of the population, related to the resources available, designated $\kappa 1$ and $\kappa 2$, respectively. **4)** For the sake of simplicity, death rates for populations x1 and x2 in the presence of antigen are assumed to be zero. However, we note that if substantial death does occur in these populations, this would be reflected in lower values for $\lambda 1$ and $\lambda 2$, and would not affect our overall conclusions.

The equations for the mathematical models that describes the populations are:

Model 1:

(i) $$\frac{dx_1(t)}{dt} = {}_1x_1(t)\ 1\ \frac{x_1(t)}{1} \div\ {}_1x_1(t)$$

(ii) $$\frac{dx_3(t)}{dt} = {}_3x_3(t) + {}_1x_1(t)$$

Model 2:

(iii) $$\frac{dx_1(t)}{dt} = {}_1x_1(t)\ 1\ \frac{x_1(t)}{1} \div\ {}_1x_1(t),$$

(iv) $$\frac{dx_2(t)}{dt} = {}_2x_2(t)\ 1\ \frac{x_2(t)}{2} \div + {}_1x_1(t)\ {}_2x_2(t),$$

(v) $$\frac{dx_3(t)}{dt} = {}_3x_3(t) + {}_2x_2(t).$$

The steady state of interest for the populations described above can be described by the following equations:

Model 1:

(iv) $x_1^* = {}_1\frac{(\quad 1 \quad 1)}{1}$,

(v) $x_3^* = \frac{{}_1 x_1^*}{3}$

Model 2:

(vi) $x_1^* = {}_1\frac{(\quad 1 \quad 1)}{1}$,

(vii) $x_2^* = \frac{2}{2\quad 2}(\quad 2 \quad 2) + \sqrt{(\quad 2 \quad 2)^2 + \frac{4\quad 1\quad 2 x_1^*}{2}}$,

(viii) $x_3^* = \frac{{}_2 x_2^*}{3}$.

We then determined a set of control parameters for the model (Table S1A). For the death rate of T_{eff} (μ3) we used 0.027 cells/day, based on the half-life of the population upon transfer into infected mice: ${}_3 = \frac{\ln(2)}{t_{1/2}(x_3)}$ (Figure 5B and 5D). We used the EdU incorporation data (Figure 4A) to estimate λ1 (self-renewal rate) and λ2 (amplification rate). (6% EdU labeling of the T_{mem} population x 24/14 hours = 0.1 cells/day for λ1 and 29% labeled x 24/14 hours = 0.5 cells/day for λ2). We set ξ1 slightly lower than λ1, and ξ2 slightly lower than λ2, to provide for stable x1 and x2 populations over time. We calculated the carrying capacities κ1 and κ2, based on the steady state equations (vi-viiii), the control parameters for λ and ξ and the mean number of x1 and x2 cells from day >40 infected mice from Figure 3. Figure 7C and 7D were generated in Mathematica (Wolfram, Champagne, IL) as a function of λ1 and ξ1 (Figure 7C) or λ2 and ξ 2 (Figure 7D). Figure 7E was generated in Python (PSF, Beaverton, OR).

To obtain a measure of the plausibility of the model and the control parameters, we performed a Bayesian statistical calibration of the model using the available data (steady state spleen T cell numbers and cell transfer data in Figure 3 and Figure 5). For the prior distributions, we used a combination of independent uniform and normal distributions that covered a wide range of possible parameter values.

To set the likelihood structure and the level of approximation, we used the following Approximate Bayesian Computation (ABC) technique (Wilkinson,

2013): 1) Randomly draw from the prior distributions for the parameters; 2) Use the chosen parameter set to simulate data from the model so we have a model prediction for every observed data point; 3) Compare the simulated data with the observed data, and retain the set of parameters if they are similar enough; 4) Repeat steps 1 to 3 until the number of retained parameter sets is large.

To compare the observed and simulated datasets, we used the following distance measure:

$$\text{(ix)} \qquad \text{Distance (Data, Simulated Data)} = \sum_{\text{Data}} \frac{\left(\text{Data - Simulated Data}\right)^2}{\text{Data}^2}$$

which is a Euclidean distance that has been scaled by the magnitude of the observed data. We say that the observed and simulated datasets are similar enough if this distance is less than 30. The resulting median values and probability functions show that the control parameters fall well within the 95% probability limits (Table S1B). Analysis was performed in Matlab (Mathworks, Natick, MA).

Code Availability

The mathematical equations for the number of cells of population x3 at steady state (Figure 7C and 7D), as a function of (model 1) $\lambda 1$ and $\xi 1$ and of (model 2) $\lambda 2$ and $\xi 2$ are provided as a Mathematica code in Supplementary File. The mathematical model to obtain the time course for the dynamics of the three populations (model 2 and Figure 7E) is provided as a numerical Python code in Supplementary File. Source code used for Bayesian statistical analysis is available upon request.

Additional Statistical Analysis for Experimental Data

All p-values were calculated using the two-tailed, unpaired Student's t test or one-way analysis of variance with Tukey's post-test according to instructions in Prism (GraphPad, La Jolla, CA). A p-value < 0.05 was considered to be statistically significant. All data met the assumptions of the test (i.e. Gaussian distribution and similar variances between groups of data being compared). Sample size in all experiments was consistent with previous experience and similar studies. No samples or animals were excluded from the analysis. The investigators were not blinded to group assessment.

AUTHOR CONTRIBUTIONS

H.H.C. designed and performed experiments, analyzed data, and wrote the manuscript. E.A.R. designed experiments, analyzed data, and wrote the manuscript. J.P.G., G.L., and C.M-P. performed mathematical modeling and statistical analyses. S-W.C., N.B., A.T., and N.S. provided critical research tools.

ACKNOWLEDGEMENTS

We thank C. Kang for generating TG6 transgenic mice, K. Taylor and I. Chou for expert technical assistance, the NIH Tetramer Core for peptide-MHC tetramers, H. Nolla and A. Valero for cell sorting, M. Jenkins (U of Minnesota), M. Prlic (Fred Hutchson Cancer Research Center), and members of the Robey Lab for helpful comments. This work was supported by grants from the American National Institutes of Health P01 AI065831 (E.A.R. and N.S.), R01 AI065537 and AI093132 (E.A.R.); the American Heart Association and the California Institute for Regenerative Medicine (H.H.C.); the Human Frontier Science Program (N.B.); the UK's National Centre for Replacement, Refinement and Reduction of Animals in Research NC/K001280/1 (J.P.G.), the Leeds Fund for International Research Collaborations (G.L. and C.M-P.), the Biotechnology and Biological Sciences Research Council BB/F003811/1 (G.L. and C.M-P.) and BB/G023395/1 (C.M-P). All authors have no competing financial interest.

REFERENCES

FIGURE LEGENDS

Figure 1: CD8+ GRA6:L^{d}-specific T cell response to *T.gondii* in genetically resistant mice exhibits immunodominance, lack of a contraction phase, and a persistent polyfunctional effector response. (A) Kinetics of parasite burden in F1 H2^{bxd} mice after oral infection with Pru strain parasites expressing RFP. Parasite loads in the mesenteric lymph node (MLN, filled circles) and in the spleen (open circles) are shown as numbers of RFP+ infected cells. Parasite loads in the brain were determined by semi-quantitative PCR. Each time point is displayed as number of parasite genomes per 1µg of brain genomic DNA (red triangles). **(B)** Representative flow cytometry plots showing GRA4:L^{d}-, ROP5:D^{b}-, or GRA6:L^{d}-tetramer expression on gated CD8+ T cells from the spleens of F1 mice day 21 after infection. Numbers represent the percent of tetramer+ cells out of total splenic CD8+ T cells. **(C)** Number of GRA4:L^{d}- (black circles), ROP5:D^{b}-

(blue circles), or GRA6:L^d-(red circles)-tetramer-specific CD8+ T cells in the spleens (top) and the brains (bottom) of infected F1 mice at the indicated time points. **(D)** *In vivo* cytotoxicity of anti-*T. gondii* CD8+ T cells. Representative histograms showing the percent of each of each target cell populations pre-transfer, or 18 hours after transfer into day 90 chronically infected mice. Target cells were individually pulsed with 1μM of indicated peptides and labeled with a different concentration of fluorescent dye, then mixed at 1:1:1:1 ratio just prior to injection into mice. Values are the percent of each donor population before and after transfer. **(E)** Left panel shows representative flow cytometry plots showing IFNγ and TNFα production of splenic CD8+ T cells from day 140 chronically infected F1 mice after *ex vivo* stimulation with indicated peptides for 4 hours. Values are the percent of IFNγ positive cells out of total CD8+ T cells. Right panel shows the percentage of TNFα producing cells amongst IFNγ+CD8+ T cells following stimulation with a serial dilution of GRA6 (red) or a mixture of GRA4 and ROP5 peptides (black). **(F)** Kinetics of surface KLRG1, CD62L, and PD-1 expression. Values are the percent positive cells out of each of the splenic GRA4:L^d-(black circles), ROP5:D^b- (blue circles), and GRA6:L^d- (red circles) tetramer+ CD8+ T cell population from mice between day 0 and day 200 post infection. Graph in **(A-C, F)** are summary of 3-5 independent experiments with total N equal to 4-10 mice at each time point. **(D, E)** are representative of 3 independent experiments with total N=5 mice 2-4 months post infection. Graphs in **(A, C and F)** display mean ±S.E.M.

Figure 2. Kinetics of antigen presentation *in vivo* correlates with GRA6:L^d-specific T cell proliferation during the chronic phase. (A) Strategy for quantification of *in vivo* GRA6 antigen levels in infected mice. (See also Experimental Procedures). **(B)** Representative flow cytometry plots of donor TG6 T cells recovered 3 days after injection into day 140 post infection mice. Control infected mice were infected with CEP strain parasites, which express an allelic form of GRA6 that lacks the relevant T cell epitope. **(C)** Compiled data showing GRA6 antigen presentation *in vivo* as measured by the proliferation of TG6 T cells recovered 3 days after transfer into mice that had been previously infected for the indicated times (red circles). Percentage of Ki67+ cells out of total endogenous splenic GRA6:L^d-tetramer+ CD8+ T cells in orally infected mice (black circles) are shown for comparison. **(D)** Representative flow cytometry plots showing Ki67 expression and 14-hour *in vivo* EdU labeling by gated splenic GRA6:L^d-specific CD8+ splenic T cells at day 15 or day 148 after infection. Panels in **(B and D)** are representative of 3 independent experiments with total N=5-6 mice per group. Graph in **(C)** is summary of 3 independent experiments with total N equal to 4-5 mice at each time point. Values are percent of cells in the indicated gates or quadrants.

Figure 3: GRA6:L^d-specific T cell immunodominance correlates with the predominance and stability of the CXCR3+KLRG1+ population. (A) Representative flow cytometry plots showing CXCR3 vs. KLRG-1 expression of splenic GRA6:L^d- and GRA4:L^d/ROP5:D^b-tetramer+ CD8+ T cells isolated at the

indicated times after infection. Naïve CD44^{low} CD8+ T cells are shown in grey for reference. **(B)** Total numbers of splenic CXCR3+KLRG1-, CXCR3+KLRG1+ and CXCR3-KLRG1+ cells within the GRA6:L^{d}- (open circles) or GRA4:L^{d}/ROP5:D^{b}- (filled circles) tetramer+ CD8+ T cells over time after infection. The dashed line indicates the detection limit of this assay at 10^3 cell/spleen. **(C)** Kinetic of total splenic donor TG6 cells (left) and number of splenic donor TG6 CXCR3+KLRG1-, CXCR3+KLRG1+ and CXCR3-KLRG1+ cells (right) after infection. Panels in **(A)** are representative of 3-6 independent experiments with total N=5-8 mice at each time point. Graphs in **(B and C)** are summary of 3-5 independent experiments with total N equal to 3-8 mice at each time point, except in **(B)**, day 140 post infection (2 independent experiment with total N equal to 2 mice). Graphs in **(B and C)** display mean±S.E.M.

Figure 4: The CXCR3+KLRG1+ subset is enriched with proliferating cells and has characteristics of both memory and effector cells. (A) Compiled scattered plots showing the percentages of Ki67+ (left), CD71+CD98+ (middle) and EdU+ (right) cells in each of the splenic GRA6:L^{d}-specific CXCR3/KLRG-1 subsets 60 days after infection. **(B)** Compiled scattered plot showing the mean fluorescent intensity (MFI) of Bcl-2 staining in each of the splenic GRA6:L^{d}-tetramer+ CXCR3/KLRG1 subsets at ≥ 40 days after infection. Data points from the same animal are indicated by connecting lines. Each symbol indicates value from individual recipients. **(C)** Representative histograms showing expression of memory/effector T cell markers CD127, CD122, CD62L, CCR7, CD27, CD43,

Blimp-1, Eomes, and T-bet in each of the splenic GRA6:L^d-specific CXCR3/KLRG-1 subsets 60 days after infection. All panels are summary of 3-6 independent experiments per group. *$P < 0.05$, **$P < 0.01$, and ***$P < 0.001$ (one-way ANOVA with Tukey's post test).

Figure 5: Lineage relationship and antigen dependence of the CXCR3/KLRG1 subsets. (A) Representative flow cytometry plots showing the CXCR3/KLRG1 phenotype and proliferation dye profile of each of the sorted donor TG6 subsets 2 days or 21 days after transfer into ≥ day 21 infected recipients. **(B)** Fold change in the number of the indicated CXCR3/KLRG1 donor-derived subsets between 2-21 days after transfer into infected recipients. Each filled circle represents the value from an individual recipient at day 21 normalized to the mean value of day 2 post transfer for that subset from all experiments. Numbers inside the graphs indicate the mean fold change for each subset between day 2 and day 21. **(C)** Representative flow cytometry plots showing the CXCR3/KLRG1 phenotype and proliferation dye profile of each of the donor TG6 subsets 2 days or 21 days after transfer of the indicated sorted subsets into naïve F1 recipient mice. **(D)** Fold change in the number of the indicated CXCR3/KLRG1 donor-derived subsets between 2-21 days after transfer into naive recipients. Each filled circle represents the value from an individual recipient at day 21 normalized to the mean value of day 2 post transfer for that subset from all experiments. Numbers inside the graphs indicate the mean fold change for each subset between day 2 and day 21. *$P < 0.05$, **$P < 0.01$, and

***$P < 0.001$ (one-way ANOVA with Tukey's post test). All panels are representative of 3-4 independent experiments. Total N of each panel is indicated in the corresponding scattered plots. **(B, D)** Half-lives of each subset ($t_{1/2}$) were calculated by: $t_{1/2} = 19\text{days} * \ln(2) / \ln(N_{day2} / N_{day21})$, N = donor TG6 cell number recovered at day 2 or day 21 post transfer.

Figure 6: Persistent antigen presentation prevents T cell contraction by sustaining the T_{int} population. (A-B) Kinetics of splenic GRA6 antigen presentation *in vivo*, as measured by proliferation of naïve TG6 T cells 3 days after transfer into infected mice (see also Figure 2A) **(A),** and splenic GRA6:L^d-tetramer+ CD8+ T cell number **(B)** in mice infected with either 10^5 live (filled circles) or 10^6 irradiated (open circles) *T. gondii* intraperitoneally. **(C)** Representative histograms showing Ki67 expression of each of the splenic GRA6:L^d-specific CXCR3/KLRG1 subsets in mice infected with 10^5 live or 10^6 irradiated *T. gondii* intraperitoneally at 12 or 21 days post infection. **(D)** Representative flow cytometry plots showing CXCR3/KLRG1 profiles of splenic GRA6:L^d-tetramer+ CD8+ T cells from mice infected with 10^5 live or 10^6 irradiated *T. gondii* intraperitoneally at 7, 12, or 21 days post infection. **(E)** (left) Kinetics of each of the splenic GRA6:L^d-tetramer+ CD8+ CXCR3/KLRG1 subsets from mice infected with 10^5 live (filled circles) or 10^6 irradiated (open circles) *T. gondii* intraperitoneally. (right) Histogram indicated the fold reduction of cell numbers in each T cell group between day 12 and 21 in mice infected with 10^6 irradiated *T. gondii*. **(F)** Kinetics of splenic ROP5 antigen presentation *in vivo* (red

circles), as measured by proliferation of naïve ROP5:D^b T cells from TR5 TCR transgenic mice 3 days after transfer into orally infected mice (see also Figure 2A.) Numbers of splenic GRA4:L^d/ROP5:D^b-specific CXCR3+KLRG1+ cells (black circle) from **Figure 3B** are shown for comparison. Right panel shows comparable data for splenic GRA6 antigen presentation *in vivo* and numbers of splenic GRA6:L^d-specific CXCR3+KLRG1+ T cells. GRA6 antigen presentation data is also displayed in **Figure 2C**, and is included here for comparison. Graph in **(A)** is summary of 2 independent experiments with total N equal to 3-4 mice at each time point. Each symbol indicates value from individual recipients. Graph in **(B)**, $*P = 0.043$ and $**P = 0.003$ (unpaired, two-tailed student t-test); Graph in **(E)**, $*P = 0.02$ (one-way ANOVA with Tukey's post test). Graphs in **(B and E)** are summary of 3-4 independent experiments with total N equal to 4-7 mice at each time point. Panels in **(C, D, and F)** are representative of 3 independent experiments with total N=3-5 mice at each time point. Graphs in **(A, B, E and F)** display mean±S.E.M.

Figure 7: Mathematical modeling illustrates the role of the amplifying T_{int} subset in maintaining a robust T_{eff} response. Mathematical models describing the population dynamics of the GRA6:L^d response with **(A)** or without **(B)** the T_{int} susbet. See also Experimental Procedures for details. **(C)** Graph showing dependence of T_{eff} cell numbers at steady state on the values of T_{mem} self-renewal rate $\lambda 1$ and differentiation rate $\xi 1$, according to model 1 in panel **(A)**. The remaining parameters were fixed at the control values (see also Table S1A).

(D) Graph showing dependence of T_{eff} cell numbers at steady state on the values of T_{int} amplification rate $\lambda 2$ and differentiation rate $\xi 2$, according to model 2 in panel **(B)**. The remaining parameters were fixed at the control values (see also Table S1A). The red dashed line indicates the experimental value for number of T_{eff} found in spleens of chronically infected mice. **(E)** Changes in number of T_{mem}, T_{int}, and T_{eff} populations as a function of time starting with 10^5 T_{mem} using the model 2 in panel **(B)** and control parameters (see also Table S1A).

References

1. Almeida, J.R., Price, D.A., Papagno, L., Arkoub, Z.A., Sauce, D., Bornstein, E., Asher, T.E., Samri, A., Schnuriger, A., Theodorou, I.*, et al.* (2007). Superior control of HIV-1 replication by CD8+ T cells is reflected by their avidity, polyfunctionality, and clonal turnover. J Exp Med *204*, 2473-2485.
2. Anderson, K.G., Mayer-Barber, K., Sung, H., Beura, L., James, B.R., Taylor, J.J., Qunaj, L., Griffith, T.S., Vezys, V., Barber, D.L., and Masopust, D. (2014). Intravascular staining for discrimination of vascular and tissue leukocytes. Nat Protoc *9*, 209-222.
3. Arens, R., and Schoenberger, S.P. (2010). Plasticity in programming of effector and memory CD8 T-cell formation. Immunol Rev *235*, 190-205.
4. Banerjee, A., Gordon, S.M., Intlekofer, A.M., Paley, M.A., Mooney, E.C., Lindsten, T., Wherry, E.J., and Reiner, S.L. (2010). Cutting edge: The transcription factor eomesodermin enables CD8+ T cells to compete for the memory cell niche. J Immunol *185*, 4988-4992.
5. Beura, L.K., Anderson, K.G., Schenkel, J.M., Locquiao, J.J., Fraser, K.A., Vezys, V., Pepper, M., and Masopust, D. (2014). Lymphocytic choriomeningitis virus persistence promotes effector-like memory differentiation and enhances mucosal T cell distribution. J Leukoc Biol.
6. Bhadra, R., Gigley, J.P., Weiss, L.M., and Khan, I.A. (2011). Control of Toxoplasma reactivation by rescue of dysfunctional CD8+ T-cell response via PD-1-PDL-1 blockade. Proc Natl Acad Sci U S A *108*, 9196-9201.
7. Blanchard, N., Gonzalez, F., Schaeffer, M., Joncker, N.T., Cheng, T., Shastri, A.J., Robey, E.A., and Shastri, N. (2008). Immunodominant, protective response to the parasite Toxoplasma gondii requires antigen processing in the endoplasmic reticulum. Nat Immunol *9*, 937-944.
8. Brown, C.R., Hunter, C.A., Estes, R.G., Beckmann, E., Forman, J., David, C., Remington, J.S., and McLeod, R. (1995). Definitive identification of a

gene that confers resistance against Toxoplasma cyst burden and encephalitis. Immunology *85*, 419-428.
9. Chtanova, T., Schaeffer, M., Han, S.-J., van Dooren, G.G., Nollmann, M., Herzmark, P., Chan, S.W., Satija, H., Camfield, K., Aaron, H.*, et al.* (2008). Dynamics of neutrophil migration in lymph nodes during infection. Immunity *29*, 487-496.
10. Demento, S.L., Cui, W., Criscione, J.M., Stern, E., Tulipan, J., Kaech, S.M., and Fahmy, T.M. (2012). Role of sustained antigen release from nanoparticle vaccines in shaping the T cell memory phenotype. Biomaterials *33*, 4957-4964.
11. Feliu, V., Vasseur, V., Grover, H.S., Chu, H.H., Brown, M.J., Wang, J., Boyle, J.P., Robey, E.A., Shastri, N., and Blanchard, N. (2013). Location of the CD8 T cell epitope within the antigenic precursor determines immunogenicity and protection against the Toxoplasma gondii parasite. PLoS Pathog *9*, e1003449.
12. Ferguson, D.J., Hutchison, W.M., and Pettersen, E. (1989). Tissue cyst rupture in mice chronically infected with Toxoplasma gondii. An immunocytochemical and ultrastructural study. Parasitol Res *75*, 599-603.
13. Frickel, E.M., Sahoo, N., Hopp, J., Gubbels, M.J., Craver, M.P., Knoll, L.J., Ploegh, H.L., and Grotenbreg, G.M. (2008). Parasite stage-specific recognition of endogenous Toxoplasma gondii-derived CD8+ T cell epitopes. J Infect Dis *198*, 1625-1633.
14. Gattinoni, L., Lugli, E., Ji, Y., Pos, Z., Paulos, C.M., Quigley, M.F., Almeida, J.R., Gostick, E., Yu, Z., Carpenito, C.*, et al.* (2011). A human memory T cell subset with stem cell-like properties. Nat Med *17*, 1290-1297.
15. Graef, P., Buchholz, V.R., Stemberger, C., Flossdorf, M., Henkel, L., Schiemann, M., Drexler, I., Hofer, T., Riddell, S.R., and Busch, D.H. (2014). Serial transfer of single-cell-derived immunocompetence reveals stemness of CD8(+) central memory T cells. Immunity *41*, 116-126.
16. Grover, H.S., Chu, H.H., Kelly, F.D., Yang, S.J., Reese, M.L., Blanchard, N., Gonzalez, F., Chan, S.W., Boothroyd, J.C., Shastri, N., and Robey, E.A. (2014). Impact of regulated secretion on antiparasitic CD8 T cell responses. Cell reports *7*, 1716-1728.
17. Hansen, S.G., Ford, J.C., Lewis, M.S., Ventura, A.B., Hughes, C.M., Coyne-Johnson, L., Whizin, N., Oswald, K., Shoemaker, R., Swanson, T.*, et al.* (2011). Profound early control of highly pathogenic SIV by an effector memory T-cell vaccine. Nature *473*, 523-527.
18. Hansen, S.G., Vieville, C., Whizin, N., Coyne-Johnson, L., Siess, D.C., Drummond, D.D., Legasse, A.W., Axthelm, M.K., Oswald, K., Trubey, C.M.*, et al.* (2009). Effector memory T cell responses are associated with protection of rhesus monkeys from mucosal simian immunodeficiency virus challenge. Nat Med *15*, 293-299.
19. Hikono, H., Kohlmeier, J.E., Takamura, S., Wittmer, S.T., Roberts, A.D., and Woodland, D.L. (2007). Activation phenotype, rather than central- or

effector-memory phenotype, predicts the recall efficacy of memory CD8+ T cells. J Exp Med *204*, 1625-1636.
20. Hiramoto, R.M., Galisteo, A.J., do Nascimento, N., and de Andrade, H.F., Jr. (2002). 200 Gy sterilised Toxoplasma gondii tachyzoites maintain metabolic functions and mammalian cell invasion, eliciting cellular immunity and cytokine response similar to natural infection in mice. Vaccine *20*, 2072-2081.
21. Hodge, R.D., Kowalczyk, T.D., Wolf, S.A., Encinas, J.M., Rippey, C., Enikolopov, G., Kempermann, G., and Hevner, R.F. (2008). Intermediate progenitors in adult hippocampal neurogenesis: Tbr2 expression and coordinate regulation of neuronal output. The Journal of neuroscience : the official journal of the Society for Neuroscience *28*, 3707-3717.
22. Hodge, R.D., Nelson, B.R., Kahoud, R.J., Yang, R., Mussar, K.E., Reiner, S.L., and Hevner, R.F. (2012). Tbr2 is essential for hippocampal lineage progression from neural stem cells to intermediate progenitors and neurons. The Journal of neuroscience : the official journal of the Society for Neuroscience *32*, 6275-6287.
23. Horton, H., Frank, I., Baydo, R., Jalbert, E., Penn, J., Wilson, S., McNevin, J.P., McSweyn, M.D., Lee, D., Huang, Y.*, et al.* (2006). Preservation of T cell proliferation restricted by protective HLA alleles is critical for immune control of HIV-1 infection. J Immunol *177*, 7406-7415.
24. International, H.I.V.C.S., Pereyra, F., Jia, X., McLaren, P.J., Telenti, A., de Bakker, P.I., Walker, B.D., Ripke, S., Brumme, C.J., Pulit, S.L.*, et al.* (2010). The major genetic determinants of HIV-1 control affect HLA class I peptide presentation. Science *330*, 1551-1557.
25. Intlekofer, A.M., Takemoto, N., Wherry, E.J., Longworth, S.A., Northrup, J.T., Palanivel, V.R., Mullen, A.C., Gasink, C.R., Kaech, S.M., Miller, J.D.*, et al.* (2005). Effector and memory CD8+ T cell fate coupled by T-bet and eomesodermin. Nat Immunol *6*, 1236-1244.
26. Jabbari, A., and Harty, J.T. (2006). Secondary memory CD8+ T cells are more protective but slower to acquire a central-memory phenotype. J Exp Med *203*, 919-932.
27. Jameson, S.C., and Masopust, D. (2009). Diversity in T cell memory: an embarrassment of riches. Immunity *31*, 859-871.
28. Joshi, N.S., Cui, W., Chandele, A., Lee, H.K., Urso, D.R., Hagman, J., Gapin, L., and Kaech, S.M. (2007). Inflammation directs memory precursor and short-lived effector CD8(+) T cell fates via the graded expression of T-bet transcription factor. Immunity *27*, 281-295.
29. Karrer, U., Sierro, S., Wagner, M., Oxenius, A., Hengel, H., Koszinowski, U.H., Phillips, R.E., and Klenerman, P. (2003). Memory inflation: continuous accumulation of antiviral CD8+ T cells over time. J Immunol *170*, 2022-2029.
30. Kohlmeier, J.E., Reiley, W.W., Perona-Wright, G., Freeman, M.L., Yager, E.J., Connor, L.M., Brincks, E.L., Cookenham, T., Roberts, A.D., Burkum, C.E.*, et al.* (2011). Inflammatory chemokine receptors regulate CD8(+) T

cell contraction and memory generation following infection. J Exp Med *208*, 1621-1634.
31. Kosmrlj, A., Read, E.L., Qi, Y., Allen, T.M., Altfeld, M., Deeks, S.G., Pereyra, F., Carrington, M., Walker, B.D., and Chakraborty, A.K. (2010). Effects of thymic selection of the T-cell repertoire on HLA class I-associated control of HIV infection. Nature *465*, 350-354.
32. Kouskoff, V., Signorelli, K., Benoist, C., and Mathis, D. (1995). Cassette vectors directing expression of T cell receptor genes in transgenic mice. J. Immunol. Methods *180*, 273-280.
33. Kraig, E., Pierce, J.L., Clarkin, K.Z., Standifer, N.E., Currier, P., Wall, K.A., and Infante, A.J. (1996). Restricted T cell receptor repertoire for acetylcholine receptor in murine myasthenia gravis. Journal of neuroimmunology *71*, 87-95.
34. Kurachi, M., Kurachi, J., Suenaga, F., Tsukui, T., Abe, J., Ueha, S., Tomura, M., Sugihara, K., Takamura, S., Kakimi, K., and Matsushima, K. (2011). Chemokine receptor CXCR3 facilitates CD8(+) T cell differentiation into short-lived effector cells leading to memory degeneration. J Exp Med *208*, 1605-1620.
35. Leon, B., Ballesteros-Tato, A., Randall, T.D., and Lund, F.E. (2014). Prolonged antigen presentation by immune complex-binding dendritic cells programs the proliferative capacity of memory CD8 T cells. J Exp Med *211*, 1637-1655.
36. Lopez, J., Bittame, A., Massera, C., Vasseur, V., Effantin, G., Valat, A., Buaillon, C., Allart, S., Fox, B.A., Rommereim, L.M.*, et al.* (2015). Intravacuolar Membranes Regulate CD8 T Cell Recognition of Membrane-Bound Toxoplasma gondii Protective Antigen. Cell reports *13*, 2273-2286.
37. Luckey, C.J., Bhattacharya, D., Goldrath, A.W., Weissman, I.L., Benoist, C., and Mathis, D. (2006). Memory T and memory B cells share a transcriptional program of self-renewal with long-term hematopoietic stem cells. Proc Natl Acad Sci U S A *103*, 3304-3309.
38. Mackay, L.K., Wakim, L., van Vliet, C.J., Jones, C.M., Mueller, S.N., Bannard, O., Fearon, D.T., Heath, W.R., and Carbone, F.R. (2012). Maintenance of T cell function in the face of chronic antigen stimulation and repeated reactivation for a latent virus infection. J Immunol *188*, 2173-2178.
39. Masopust, D., Ha, S.J., Vezys, V., and Ahmed, R. (2006). Stimulation history dictates memory CD8 T cell phenotype: implications for prime-boost vaccination. J Immunol *177*, 831-839.
40. Masopust, D., and Picker, L.J. (2012). Hidden memories: frontline memory T cells and early pathogen interception. J Immunol *188*, 5811-5817.
41. Montoya, J.G., and Liesenfeld, O. (2004). Toxoplasmosis. Lancet *363*, 1965-1976.
42. Narayanan, S., and Kranz, D.M. (2013). The same major histocompatibility complex polymorphism involved in control of HIV influences peptide binding in the mouse H-2Ld system. J Biol Chem *288*, 31784-31794.

43. Nelson, R.W., McLachlan, J.B., Kurtz, J.R., and Jenkins, M.K. (2013). CD4+ T cell persistence and function after infection are maintained by low-level peptide:MHC class II presentation. J Immunol *190*, 2828-2834.
44. Olson, J.A., McDonald-Hyman, C., Jameson, S.C., and Hamilton, S.E. (2013). Effector-like CD8(+) T cells in the memory population mediate potent protective immunity. Immunity *38*, 1250-1260.
45. Paley, M.A., Kroy, D.C., Odorizzi, P.M., Johnnidis, J.B., Dolfi, D.V., Barnett, B.E., Bikoff, E.K., Robertson, E.J., Lauer, G.M., Reiner, S.L., and Wherry, E.J. (2012). Progenitor and terminal subsets of CD8+ T cells cooperate to contain chronic viral infection. Science *338*, 1220-1225.
46. Rohr, J.C., Gerlach, C., Kok, L., and Schumacher, T.N. (2014). Single cell behavior in T cell differentiation. Trends Immunol *35*, 170-177.
47. Sallusto, F., Lenig, D., Forster, R., Lipp, M., and Lanzavecchia, A. (1999). Two subsets of memory T lymphocytes with distinct homing potentials and effector functions. Nature *401*, 708-712.
48. Shah, S., Grotenbreg, G.M., Rivera, A., and Yap, G.S. (2015). An extrafollicular pathway for the generation of effector CD8(+) T cells driven by the proinflammatory cytokine, IL-12. Elife *4*.
49. Simonetta, F., Hua, S., Lecuroux, C., Gerard, S., Boufassa, F., Saez-Cirion, A., Pancino, G., Goujard, C., Lambotte, O., Venet, A., and Bourgeois, C. (2014). High eomesodermin expression among CD57+ CD8+ T cells identifies a CD8+ T cell subset associated with viral control during chronic human immunodeficiency virus infection. J Virol *88*, 11861-11871.
50. Snyder, C.M., Cho, K.S., Bonnett, E.L., Allan, J.E., and Hill, A.B. (2011). Sustained CD8+ T cell memory inflation after infection with a single-cycle cytomegalovirus. PLoS Pathog *7*, e1002295.
51. Snyder, C.M., Cho, K.S., Bonnett, E.L., van Dommelen, S., Shellam, G.R., and Hill, A.B. (2008). Memory inflation during chronic viral infection is maintained by continuous production of short-lived, functional T cells. Immunity *29*, 650-659.
52. Torti, N., Walton, S.M., Brocker, T., Rulicke, T., and Oxenius, A. (2011). Non-hematopoietic cells in lymph nodes drive memory CD8 T cell inflation during murine cytomegalovirus infection. PLoS Pathog *7*, e1002313.
53. Turner, D.L., Cauley, L.S., Khanna, K.M., and Lefrancois, L. (2007). Persistent antigen presentation after acute vesicular stomatitis virus infection. J Virol *81*, 2039-2046.
54. Vezys, V., Masopust, D., Kemball, C.C., Barber, D.L., O'Mara, L.A., Larsen, C.P., Pearson, T.C., Ahmed, R., and Lukacher, A.E. (2006). Continuous recruitment of naive T cells contributes to heterogeneity of antiviral CD8 T cells during persistent infection. J Exp Med *203*, 2263-2269.
55. Vidal, S.M., and Lanier, L.L. (2006). NK cell recognition of mouse cytomegalovirus-infected cells. Curr Top Microbiol Immunol *298*, 183-206.
56. Virgin, H.W., Wherry, E.J., and Ahmed, R. (2009). Redefining chronic viral infection. Cell *138*, 30-50.

57. Wakim, L.M., Woodward-Davis, A., and Bevan, M.J. (2010). Memory T cells persisting within the brain after local infection show functional adaptations to their tissue of residence. Proc Natl Acad Sci U S A *107*, 17872-17879.
58. Watkins, D.I., Burton, D.R., Kallas, E.G., Moore, J.P., and Koff, W.C. (2008). Nonhuman primate models and the failure of the Merck HIV-1 vaccine in humans. Nat Med *14*, 617-621.
59. Wherry, E., Teichgraber, V., Becker, T., Masopust, D., Kaech, S., Antia, R., von Andrian, U., and Ahmed, R. (2003). Lineage relationship and protective immunity of memory CD8 T cell subsets. Nat. Immunol. *4*, 225-234.
60. Wherry, E.J. (2011). T cell exhaustion. Nat Immunol *12*, 492-499.
61. Wilkinson, R.D. (2013). Approximate Bayesian computation (ABC) gives exact results under the assumption of model error. Statistical applications in genetics and molecular biology *12*, 129-141.
62. Zehn, D., Lee, S., and Bevan, M. (2009). Complete but curtailed T-cell response to very low-affinity antigen. Nature *458*, 211-214.

Figure 1

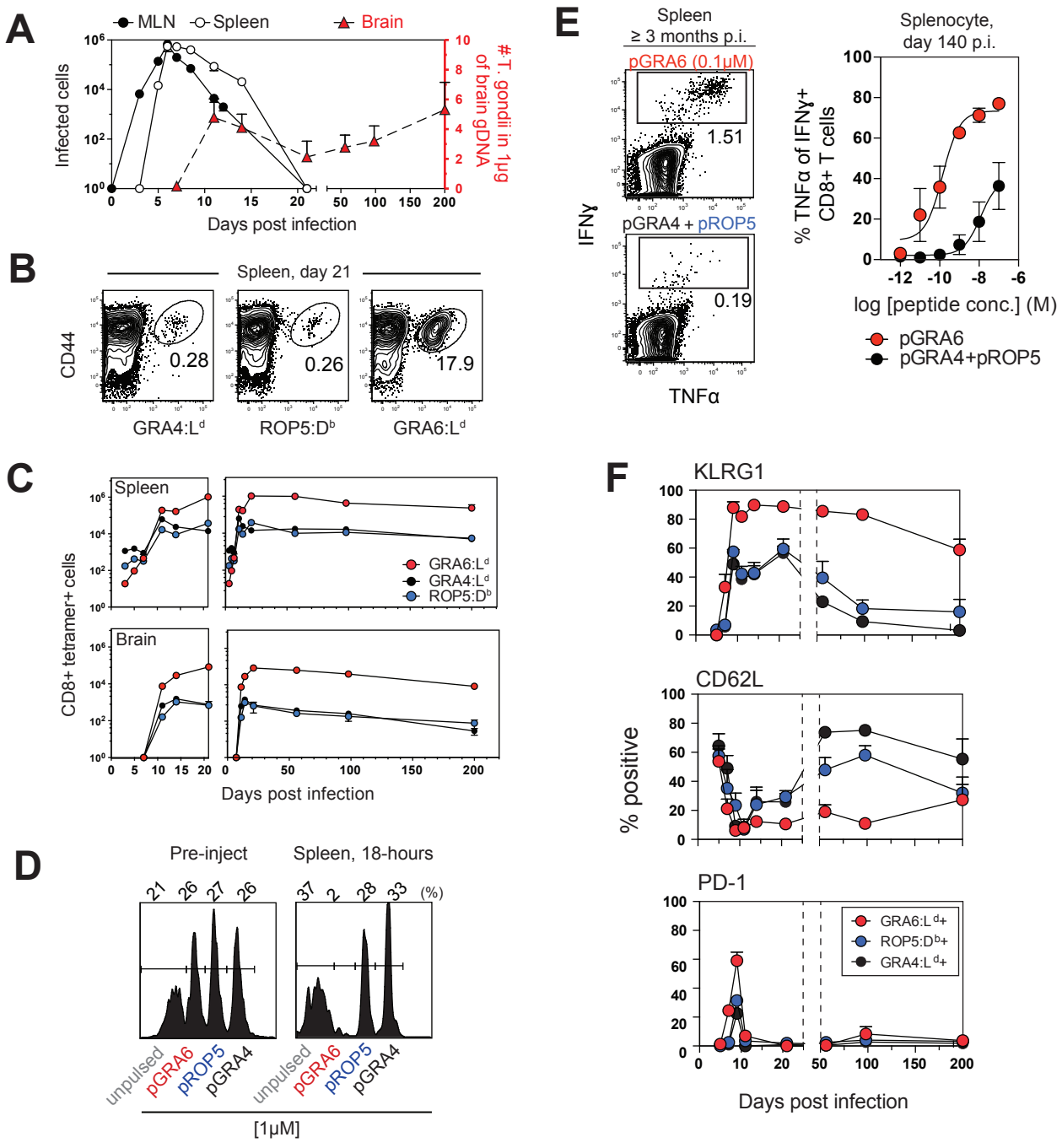
A
MLN
Spleen
Brain
Infected cells
#T. gondii in 1µg of brain gDNA
Days post infection
B
Spleen, day 21
CD44
0.28
0.26
17.9
GRA4:Ld
ROP5:Db
GRA6:Ld
C
Spleen
Brain
CD8+ tetramer+ cells
GRA6:Ld
GRA4:Ld
ROP5:Db
Days post infection
D
Pre-inject
Spleen, 18-hours
21 26 27 26
37 2 28 33 (%)
unpulsed
pGRA6
pROP5
pGRA4
[1µM]
E
Spleen
≥ 3 months p.i.
pGRA6 (0.1µM)
1.51
pGRA4 + pROP5
0.19
IFNγ
TNFα
Splenocyte,
day 140 p.i.
% TNFα of IFNγ+ CD8+ T cells
log [peptide conc.] (M)
pGRA6
pGRA4+pROP5
F
KLRG1
CD62L
PD-1
% positive
GRA6:Ld+
ROP5:Db+
GRA4:Ld+
Days post infection

Figure 2

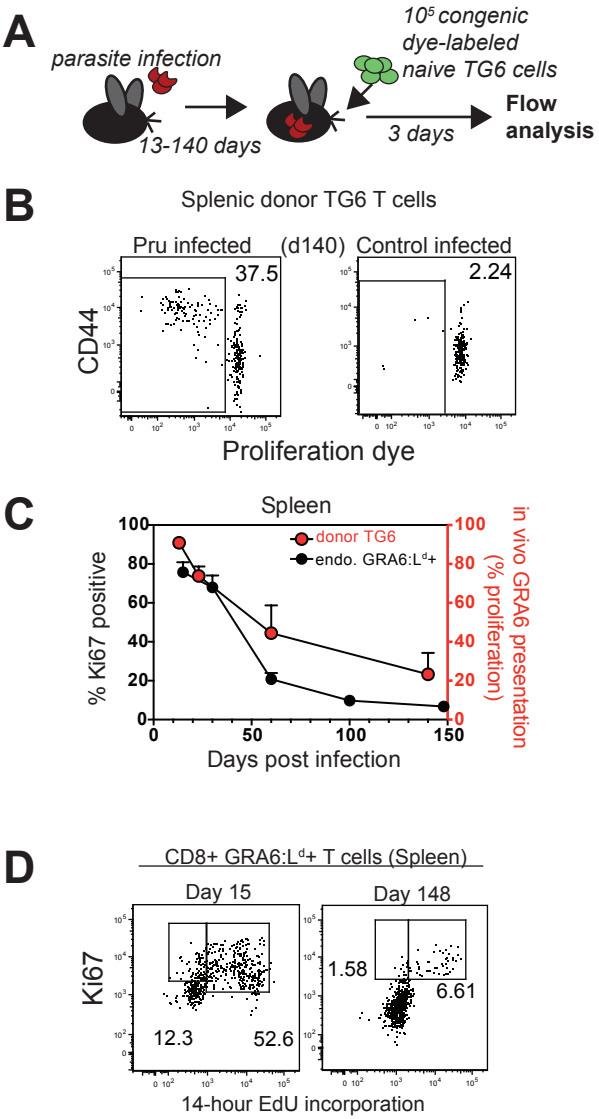
A
parasite infection
13-140 days
10⁵ congenic
dye-labeled
naive TG6 cells
3 days
Flow
analysis
B
Splenic donor TG6 T cells
Pru infected (d140)
Control infected
37.5
2.24
CD44
Proliferation dye
C
Spleen
donor TG6
endo. GRA6:Ld+
% Ki67 positive
in vivo GRA6 presentation
(% proliferation)
Days post infection
D
CD8+ GRA6:Ld+ T cells (Spleen)
Day 15
Day 148
Ki67
12.3
52.6
1.58
6.61
14-hour EdU incorporation

Figure 3

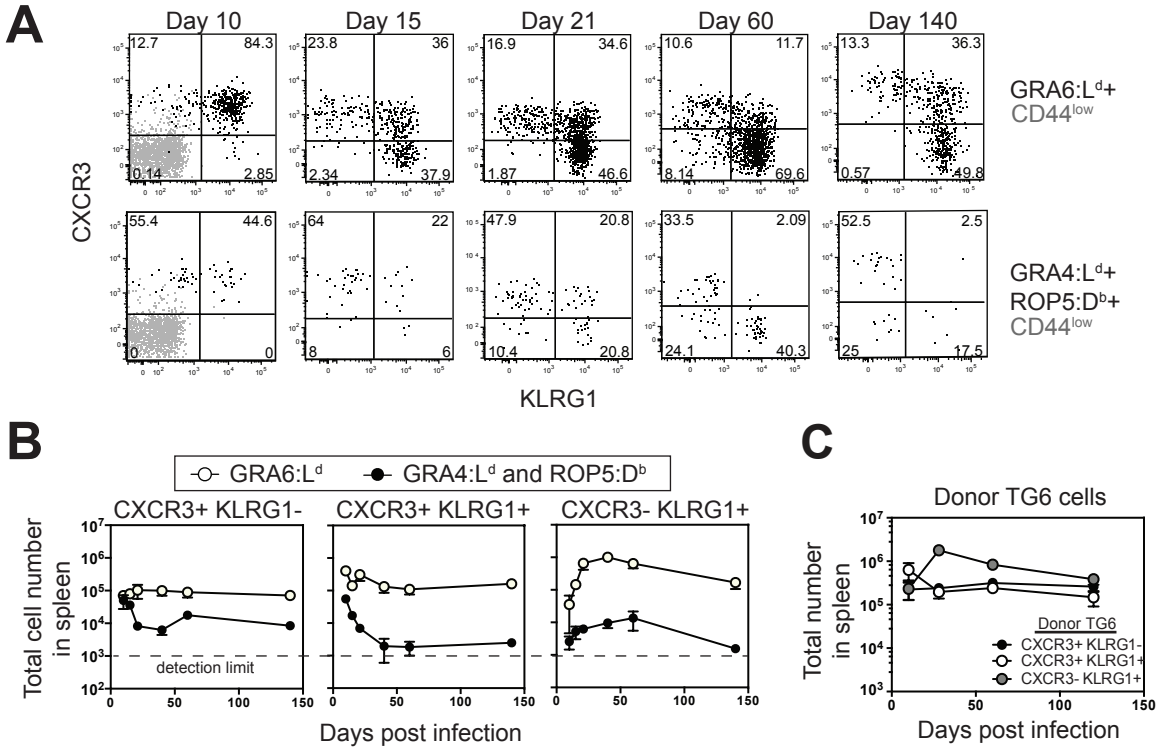
A
Day 10
Day 15
Day 21
Day 60
Day 140
CXCR3
KLRG1
GRA6:L^d+ CD44^low
GRA4:L^d+ ROP5:D^b+ CD44^low
B
GRA6:L^d
GRA4:L^d and ROP5:D^b
CXCR3+ KLRG1-
CXCR3+ KLRG1+
CXCR3- KLRG1+
Total cell number in spleen
detection limit
Days post infection
C
Donor TG6 cells
Total number in spleen
Donor TG6
CXCR3+ KLRG1-
CXCR3+ KLRG1+
CXCR3- KLRG1+
Days post infection

Figure 4

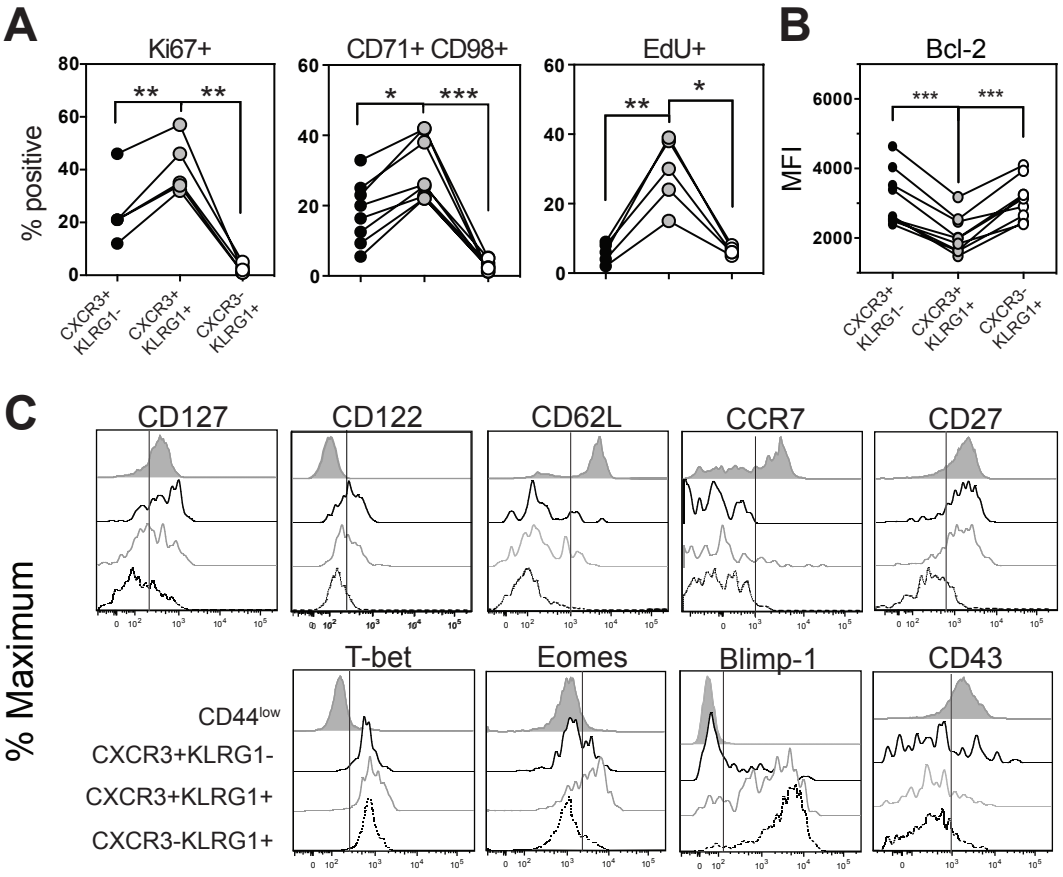
A
Ki67+
CD71+ CD98+
EdU+
% positive
B
Bcl-2
MFI
CXCR3+ KLRG1-
CXCR3+ KLRG1+
CXCR3- KLRG1+
C
CD127
CD122
CD62L
CCR7
CD27
T-bet
Eomes
Blimp-1
CD43
% Maximum
CD44low
CXCR3+KLRG1-
CXCR3+KLRG1+
CXCR3-KLRG1+

Figure 5

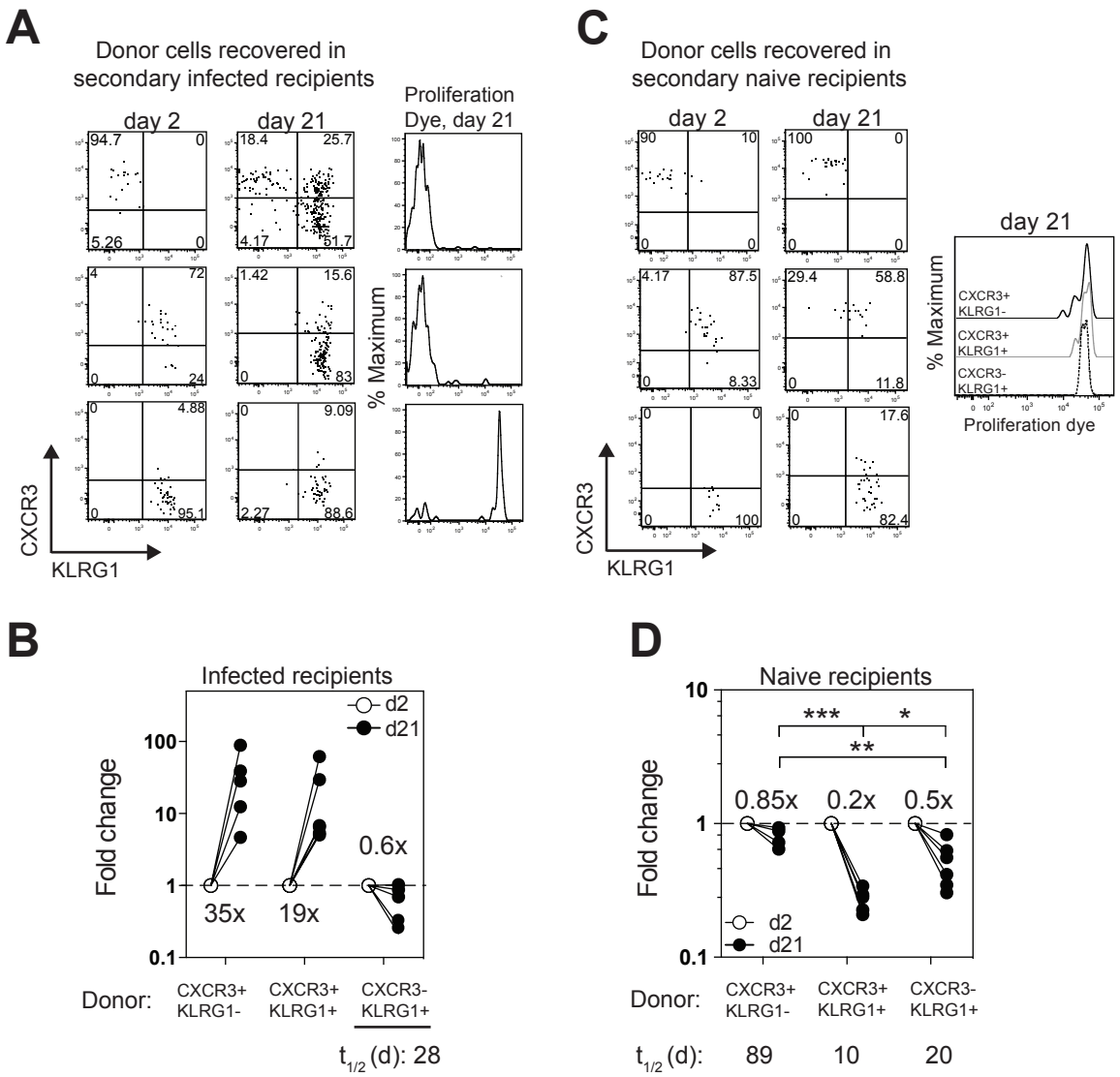
A
Donor cells recovered in secondary infected recipients
day 2
day 21
Proliferation Dye, day 21
94.7
0
5.26
0
18.4
25.7
4.17
51.7
4
72
0
24
1.42
15.6
0
83
0
4.88
0
95.1
0
9.09
2.27
88.6
% Maximum
CXCR3
KLRG1
C
Donor cells recovered in secondary naive recipients
day 2
day 21
90
10
0
0
100
0
0
0
4.17
87.5
0
8.33
29.4
58.8
0
11.8
0
0
0
100
0
17.6
0
82.4
CXCR3
KLRG1
day 21
CXCR3+ KLRG1-
CXCR3+ KLRG1+
CXCR3- KLRG1+
% Maximum
Proliferation dye
B
Infected recipients
d2
d21
Fold change
100
10
1
0.1
35x
19x
0.6x
Donor:
CXCR3+ KLRG1-
CXCR3+ KLRG1+
CXCR3- KLRG1+
t1/2 (d): 28
D
Naive recipients
10
1
0.1
***
*
**
0.85x
0.2x
0.5x
Fold change
d2
d21
Donor:
CXCR3+ KLRG1-
CXCR3+ KLRG1+
CXCR3- KLRG1+
t1/2 (d):
89
10
20

Figure 6

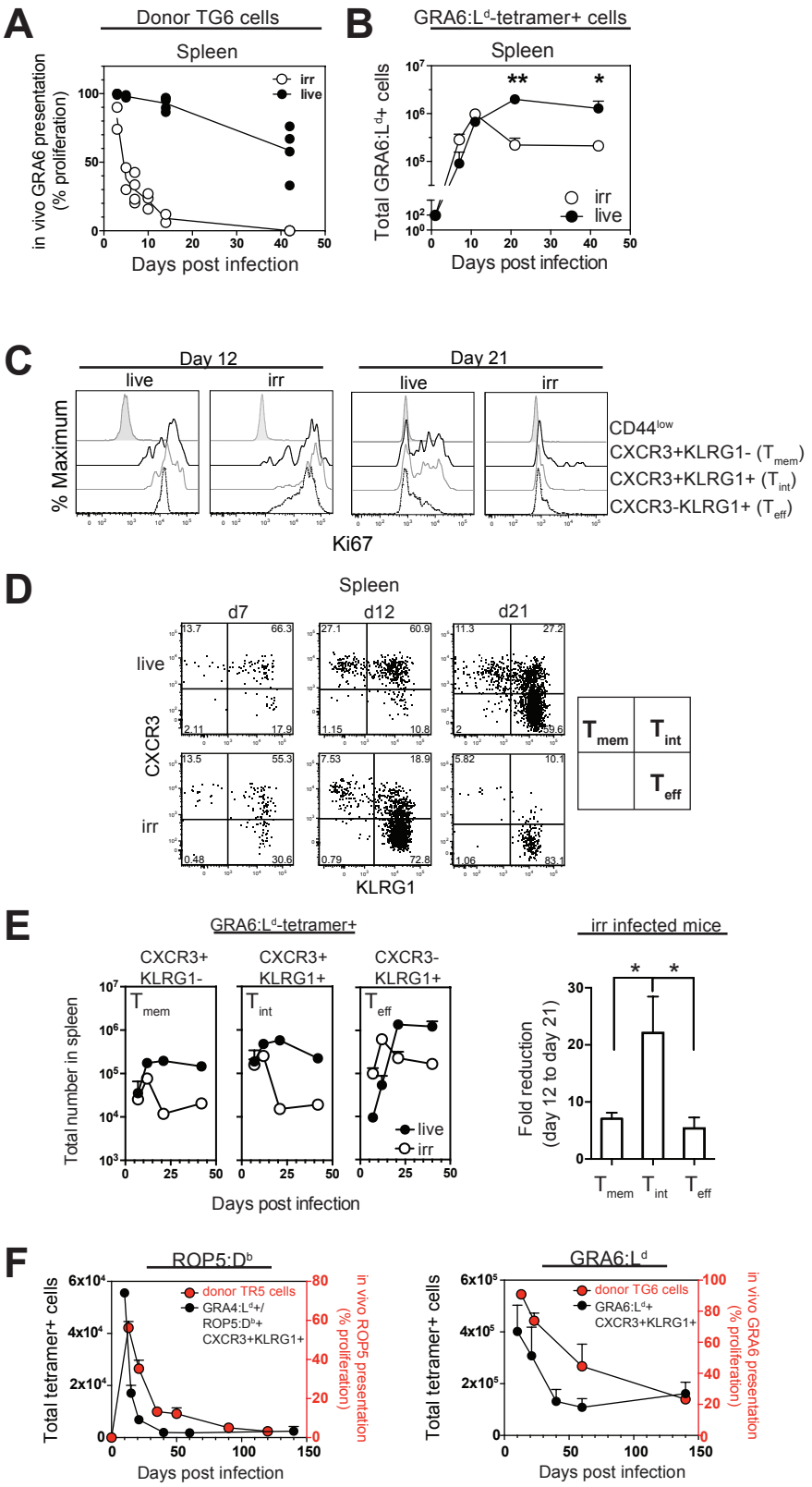
A
Donor TG6 cells
Spleen
in vivo GRA6 presentation (% proliferation)
irr
live
Days post infection
B
GRA6:Ld-tetramer+ cells
Spleen
Total GRA6:Ld+ cells
**
*
irr
live
Days post infection
C
Day 12
Day 21
live
irr
% Maximum
CD44low
CXCR3+KLRG1- (Tmem)
CXCR3+KLRG1+ (Tint)
CXCR3-KLRG1+ (Teff)
Ki67
D
Spleen
d7
d12
d21
live
irr
CXCR3
KLRG1
Tmem
Tint
Teff
E
GRA6:Ld-tetramer+
CXCR3+ KLRG1-
CXCR3+ KLRG1+
CXCR3- KLRG1+
Tmem
Tint
Teff
Total number in spleen
live
irr
Days post infection
irr infected mice
Fold reduction (day 12 to day 21)
F
ROP5:Db
donor TR5 cells
GRA4:Ld+/ ROP5:Db+ CXCR3+KLRG1+
Total tetramer+ cells
in vivo ROP5 presentation (% proliferation)
Days post infection
GRA6:Ld
donor TG6 cells
GRA6:Ld+ CXCR3+KLRG1+
Total tetramer+ cells
in vivo GRA6 presentation (% proliferation)
Days post infection

Figure 7

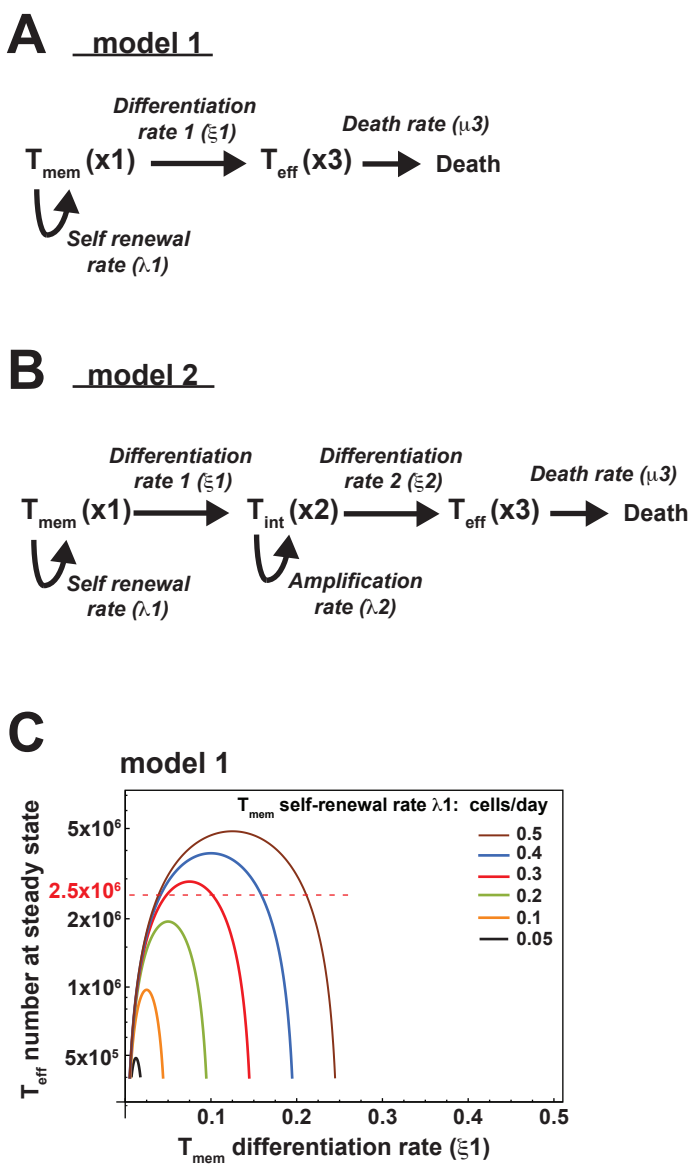
A
model 1
Differentiation rate 1 (ξ1)
Death rate (μ3)
T mem (x1)
T eff (x3)
Death
Self renewal rate (λ1)
B
model 2
Differentiation rate 1 (ξ1)
Differentiation rate 2 (ξ2)
Death rate (μ3)
T mem (x1)
T int (x2)
T eff (x3)
Death
Self renewal rate (λ1)
Amplification rate (λ2)
C
model 1
T mem self-renewal rate λ1: cells/day
0.5
0.4
0.3
0.2
0.1
0.05
5x10^6
2.5x10^6
2x10^6
1x10^6
5x10^5
T eff number at steady state
0.1
0.2
0.3
0.4
0.5
T mem differentiation rate (ξ1)
D
model 2
(λ1 = 0.1; ξ1 = 0.09 cells/day)
T int amplification rate λ2: cells/day
2.0
1.0
0.5
0.2
0.1
0.02
1x10^7
5x10^6
2.5x10^6
1x10^6
5x10^5
T eff number at steady state
0.5
1.0
1.5
2.0
2.5
3.0
T int differentiation rate (ξ2)
E
model 2
10^7
10^6
10^5
10^4
10^3
10^2
10^1
0
number of cells
T mem (CXCR3+ KLRG1-)
T int (CXCR3+ KLRG1+)
T eff (CXCR3- KLRG1+)
0
10
20
30
40
50
60
Time (days)

Figure S1

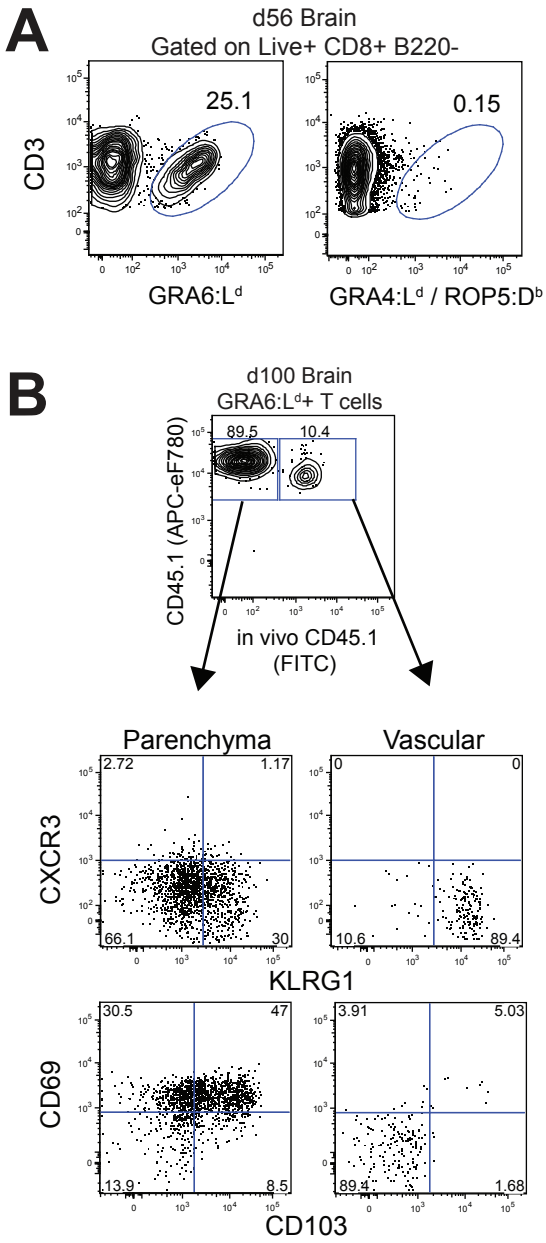

Figure S2

A **TG6 TCR (GRA6:L^d-specific)**

TCR-alpha:

- TRAV6-7/DV9*01, TRAJ52*01
- CDR3: **CALGDPTGANTGKLTF**

TCR-beta:

- TRBV1*01,TRBD1*01 TRBJ2-1*01
- CDR3: **CTCSAGRGGYAEQFF**

B

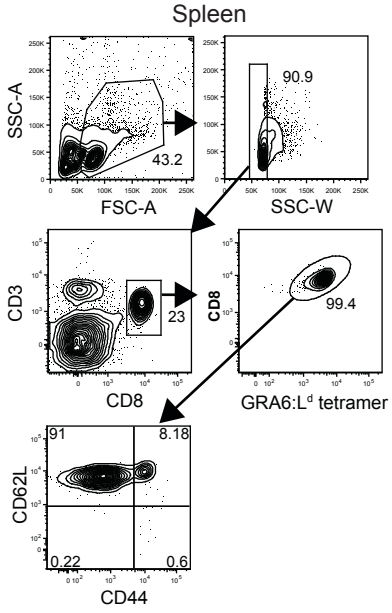

Figure S3

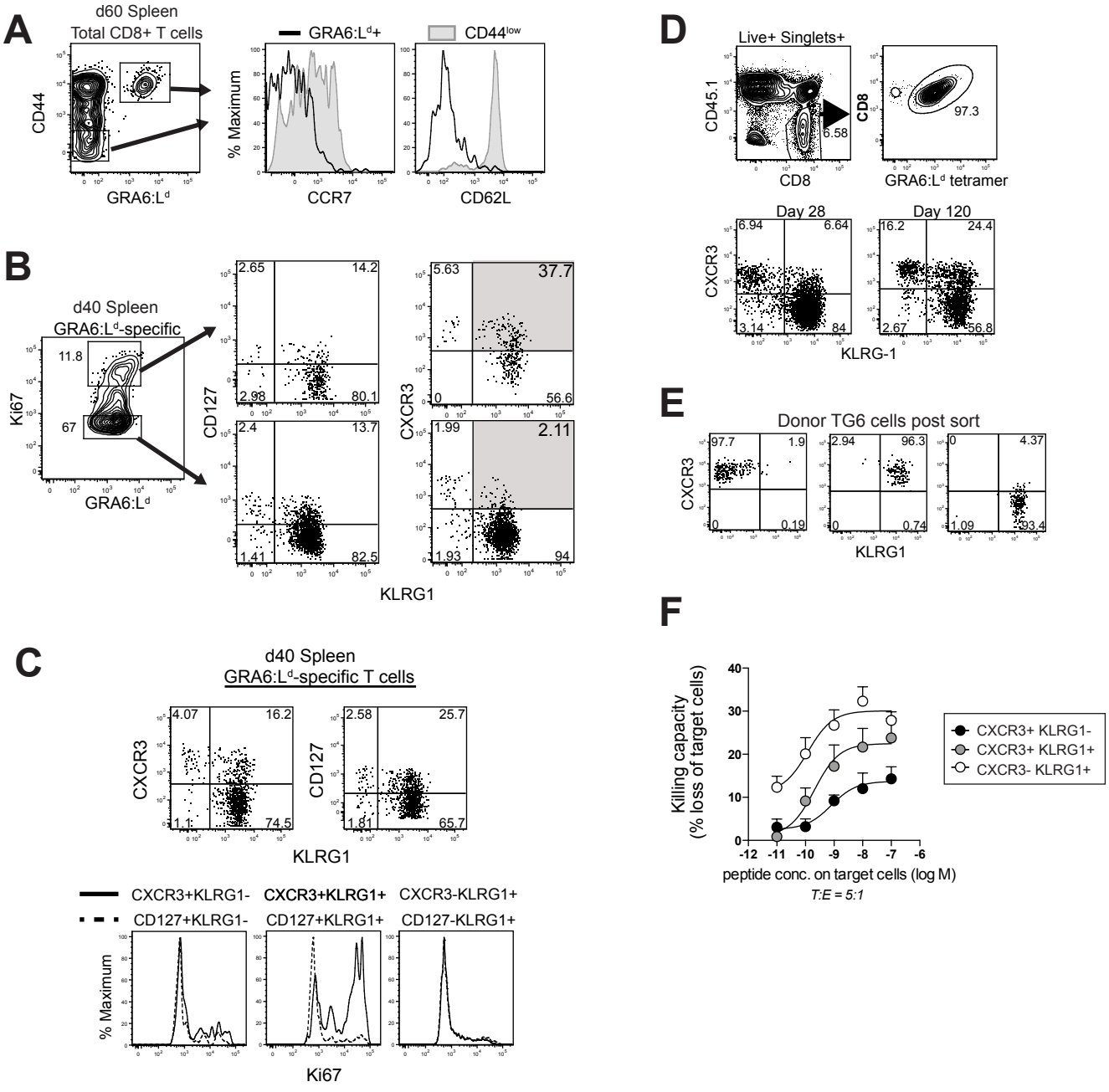
A
d60 Spleen
Total CD8+ T cells
CD44
GRA6:Ld
GRA6:Ld+
CD44low
% Maximum
CCR7
CD62L
B
d40 Spleen
GRA6:Ld-specific
11.8
67
Ki67
GRA6:Ld
2.65
14.2
2.98
80.1
2.4
13.7
1.41
82.5
CD127
5.63
37.7
0
56.6
1.99
2.11
1.93
94
CXCR3
KLRG1
C
d40 Spleen
GRA6:Ld-specific T cells
4.07
16.2
1.1
74.5
CXCR3
2.58
25.7
1.61
65.7
CD127
KLRG1
CXCR3+KLRG1-
CXCR3+KLRG1+
CXCR3-KLRG1+
CD127+KLRG1-
CD127+KLRG1+
CD127-KLRG1+
% Maximum
Ki67
D
Live+ Singlets+
CD45.1
6.58
CD8
97.3
GRA6:Ld tetramer
Day 28
Day 120
CXCR3
6.94
6.64
3.14
84
16.2
24.4
2.67
56.8
KLRG-1
E
Donor TG6 cells post sort
CXCR3
97.7
1.9
0
0.19
2.94
96.3
0
0.74
0
4.37
1.09
93.4
KLRG1
F
Killing capacity
(% loss of target cells)
40
30
20
10
0
-12
-11
-10
-9
-8
-7
-6
peptide conc. on target cells (log M)
T:E = 5:1
CXCR3+ KLRG1-
CXCR3+ KLRG1+
CXCR3- KLRG1+

Figure S4

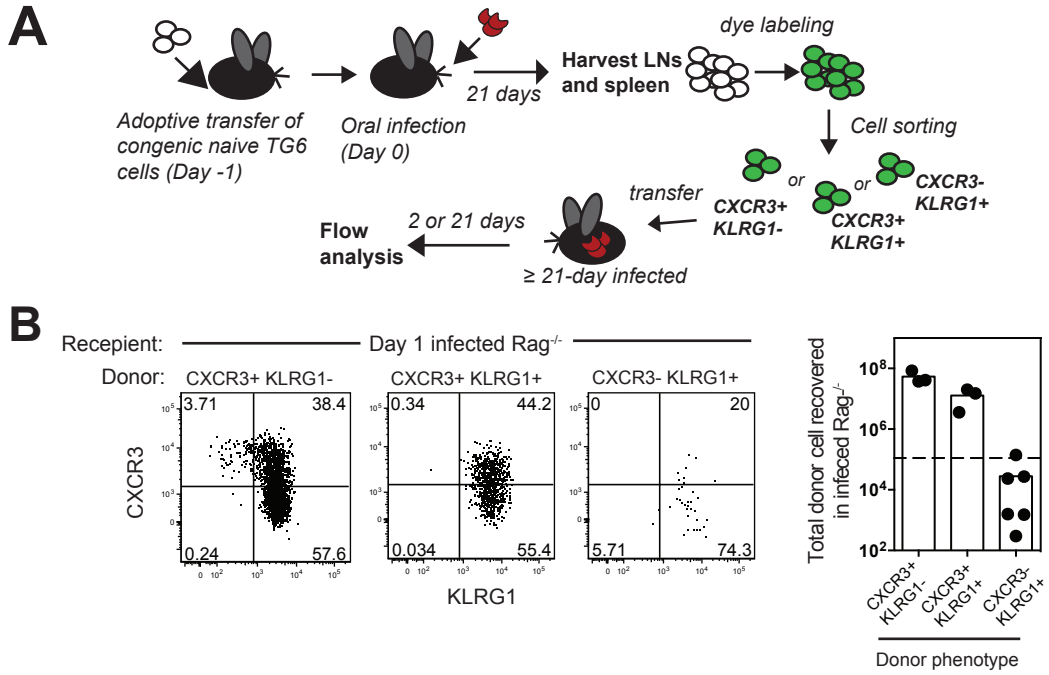
A
Adoptive transfer of congenic naive TG6 cells (Day -1)
Oral infection (Day 0)
21 days
Harvest LNs and spleen
dye labeling
Cell sorting
CXCR3+ KLRG1-
or
CXCR3+ KLRG1+
or
CXCR3- KLRG1+
transfer
≥ 21-day infected
2 or 21 days
Flow analysis
B
Recepient:
Day 1 infected Rag-/-
Donor:
CXCR3+ KLRG1-
CXCR3+ KLRG1+
CXCR3- KLRG1+
CXCR3
KLRG1
3.71
38.4
0.24
57.6
0.34
44.2
0.034
55.4
0
20
5.71
74.3
Total donor cell recovered in infeced Rag-/-
CXCR3+ KLRG1-
CXCR3+ KLRG1+
CXCR3- KLRG1+
Donor phenotype

Figure S5

A **TR5 TCR (ROP5:D^b-specific)**

TCR-alpha:

- TRAV10*02, TRAJ49*01
- CDR3: **CAARPYTGYQNFYF**

TCR-beta:

- TRBV13.3*01,TRBD1*01 TRBJ2-5*01
- CDR3: **CASSDGDTQYF**

B

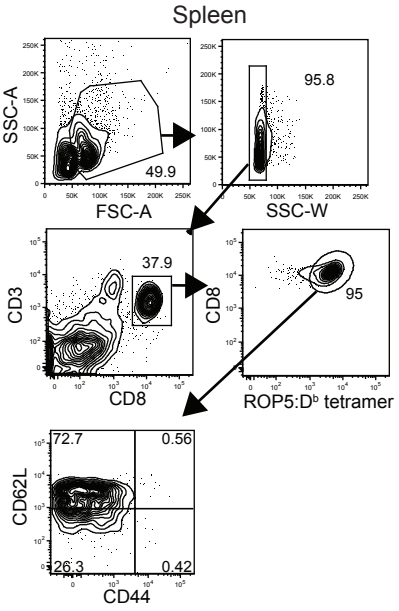

Figure S6

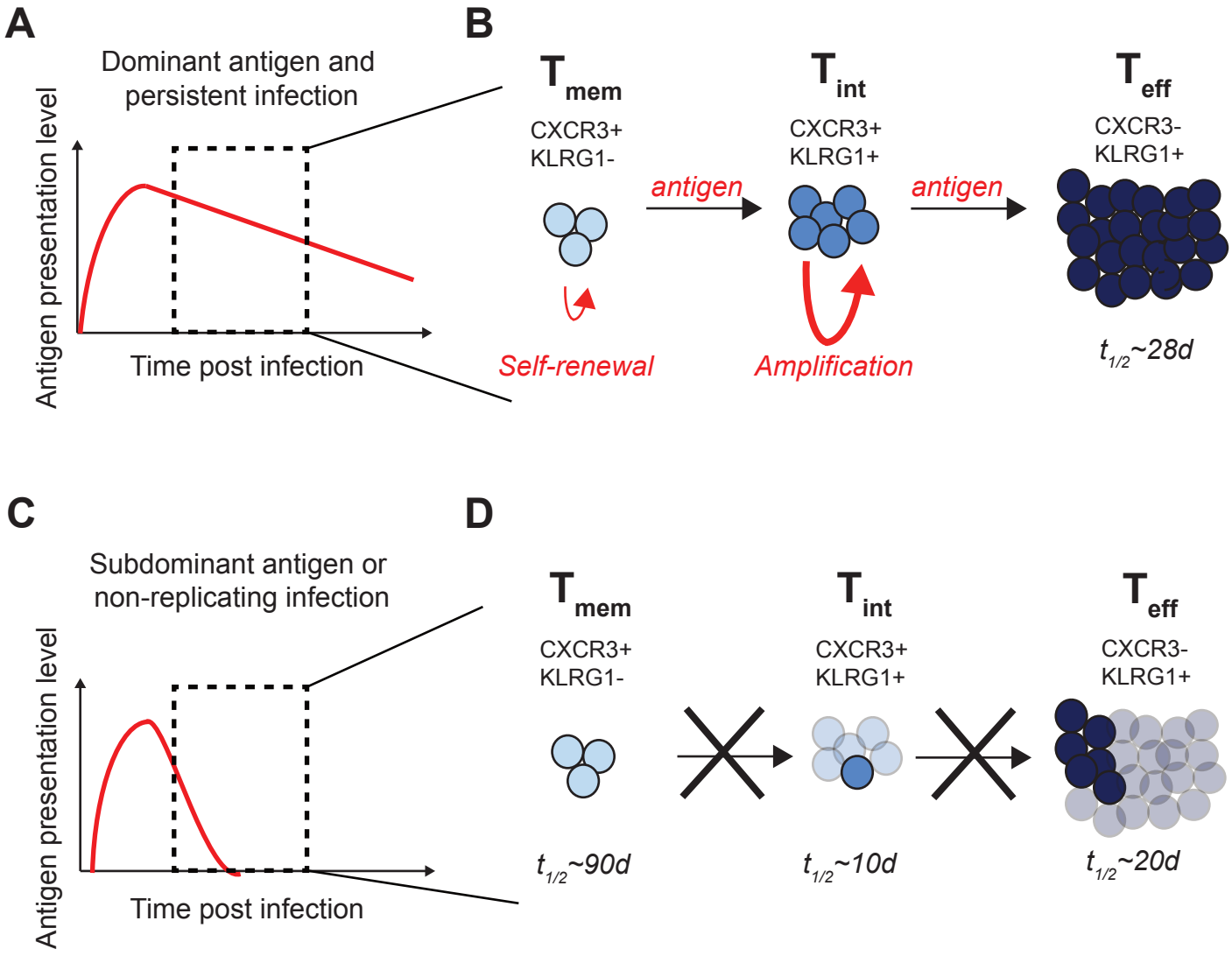
A
Dominant antigen and
persistent infection
Antigen presentation level
Time post infection
B
T mem
CXCR3+
KLRG1-
antigen
T int
CXCR3+
KLRG1+
antigen
T eff
CXCR3-
KLRG1+
Self-renewal
Amplification
t1/2~28d
C
Subdominant antigen or
non-replicating infection
Antigen presentation level
Time post infection
D
T mem
CXCR3+
KLRG1-
T int
CXCR3+
KLRG1+
T eff
CXCR3-
KLRG1+
t1/2~90d
t1/2~10d
t1/2~20d

Figure S1. Related to Figure 1. Phenotype of brain resident GRA6:L^d-specific T cells in chronically infected mice. (A) Representative flow cytometry plots showing the percentage of GRA6:L^d (Left) or GRA4:L^d+ROP5:D^b (Right) -specific T cells out of total CD8+ T cells in the brain of day 56 orally infected mice. **(B)** Representative flow cytometry plots showing surface expression of CXCR3, KLRG1, CD69 and CD103 on brain parenchyma (CD45.1-) and vascular –associated (CD45.1+) GRA6:Ld-specific T cells from day 100 orally infected CD45.1+ mice. Mice were injected i.v. with FITC-conjugated CD45.1 antibodies just prior to sacrifice to label blood-exposed lymphocytes.

Figure S2. Related to Figure 3. Characterization of the GRA6:L^d-specific TCR transgenic (TG6) mice. (A) TCR alpha and beta chain information of the GRA6:L^d-specific TCR used to create the TG6 transgenic mice. **(B)** Representative flow cytometry plots showing the TCR expression and phenotype of splenocytes of the TG6 mice. Panel **(B)** is representative of 5 independent experiments with total N=8 mice per group. Values are percent of cells in the indicated gates or quadrants.

Figure S3. Related to Figure 3 and Figure 4. CXCR3 and KLRG1, but not other commonly used memory/effector markers, identify a proliferative subset within the antigen-experienced GRA6:L^d-specific T cells during chronic infection. (A) Representative histograms showing CCR7 and CD62L expression on GRA6:L^d-specific CD8+ splenic T cells (solid line) and total

$CD44^{low}$ CD8+ T cells (shaded) in orally infected mice 60 days post infection. **(B)** Representative flow cytometry plots showing the frequencies of subsets gated based on CD127/KLRG1 expression and CXCR3/KLRG1 expression in $Ki67^{high}$ or $Ki67^{neg}$ GRA6:L^d-specific CD8+ splenic T cells in orally infected mice 40 days post infection. **(C)** Representative histograms comparing the Ki67 expression between each of CD127/KLRG1 (dotted line) and CXCR3/KLRG1 (solid line) subsets in GRA6:L^d-specific CD8+ splenic T cells in orally infected mice 40 days post infection. **(D)** Representative flow cytometry plots showing phenotypes of TG6 T cells after infection. Twenty-thousand naive CD45.2+ TG6 T cells were transferred into naïve CD45.1+ F1 mice one day before infection. CXCR3 and KLRG1 expression of donor TG6 cells were examined 28 days and 120 days after infection. **(E)** Representative flow cytometry plots showing the post sort purity of individual TG6 CXCR3/KLRG1 subsets after 28 days of infection. **(F)** *in vitro* cytotoxicity of TG6 T cell subsets. Each subset was cultured with GRA6-peptide pulsed splenocytes at 1:5:5 ratio. Splenocytes were harvested at day 1 post culture. Killing capacity indicates the percent loss of the GRA6-pulsed splenocytes relative to unlabeled target cell control. Panels in (A, B,and C) are representative of 3 independent experiments with total N=3-6 mice per group. Panels in **(D, E and F)** are representative of 10, 8 and 3 independent experiments respectively. Values are percent of cells in the indicated gates or quadrants. Graph in **(F)** display mean ±S.E.M. Nonlinear regression with least-square fitting method was used to determine best-fit curves. Values are percent of cells in the indicated gates or quadrants.

Figure S4. Related to Figure 5. Lineage tracing of the TG6 CXCR3/KLRG1 subsets. (A) Experimental design. **(B)** Representative flow cytometry plots showing the CXCR3/KLRG1 phenotype of each of the sorted donor TG6 subsets 8 days after transfer into F1 *rag*$^{-/-}$ recipients infected 1 day before transfer (left). Total donor cell number recovered from each recipient is shown in the histogram (right). Horizontal line indicates the number of donor cells transferred. Each symbol indicates value from individual recipients. Panels are summary of 2-3 independent experiments per group. Total N = 3 or 6 recipients per group.

Figure S5. Related to Figure 6. Characterization of the ROP5:D^{b}-specific TCR transgenic (TR5) mice. (A) TCR alpha and beta chain information of the ROP5:D^{b}-specific TCR used to create the TR5 transgenic mice. **(B)** Representative flow cytometry plots showing the TCR expression and phenotype of splenocytes of the TR5 mice. Panel **(B)** is representative of 3 independent experiments with total N=5 mice per group. Values are percent of cells in the indicated gates or quadrants.

Figure S6. Related to Figure 7. Schematic of the cellular mechanism that maintains the GRA6:L^{d} T cell response in persistently infected, resistant mice. (A) After the initial control of acute infection, the levels of *in vivo* presentation of GRA6 antigen decline relatively slowly. **(B)** Persistent antigen presentation during chronic infection supports low-level proliferation of T_{mem} cells and their differentiation into rapidly proliferating T_{int} cells. Antigen presentation

supports the proliferation of T_{int} cells and drives their differentiation into T_{eff} cells. Production of new T_{eff} via the T_{int} population occurs at a rate that balances their death rate, so that the steady state levels of T_{eff} remain high throughout infection. **(C)** Antigen presentation drops more sharply for subdominant antigens, or when parasites cannot replicate. **(D)** In the absence of antigen presentation, T_{mem} cells are relatively long-lived, but no longer divide or differentiate. T_{int} cells die rapidly and cease to differentiate into T_{eff} cells in the absence of antigen presentation, leading to the contraction of the T cell response. The estimated *in vivo* half-life ($t_{1/2}$) for each non-replicating population is indicated.

Table S1. Related to Figure 7.

A. Control parameters for Figure 7C, D and E.

Parameters	μ_3	λ_1	λ_2	ξ_1	ξ_2	κ_1	κ_2	x_1
Control Values	0.027	0.1	0.5	0.09	0.4	1.05×10^6	4.60×10^5	10^5
units	/days	/days	/days	/days	cells	cells	cells	cells

B. Preliminary Bayesian Study

Parameters	μ_3	λ_1	λ_2	ξ_1	ξ_2	κ_1	κ_2
Posterior median	0.05	0.4	0.46	1.97	2.28	4.72×10^6	5.00×10^6
Posterior 2.5th	0.01	0.02	0.02	0.21	0.31	1.96×10^5	2.04×10^5
Posterior 97.5th	0.09	1.66	1.81	3.91	3.92	9.70×10^6	9.76×10^6
units	/days	/days	/days	/days	cells	cells	cells

Table S1. Parameters for GRA6:L^d-specific T cell differentiation modeling during chronic phase. (A) Control parameters used to construct Figure 7C, 7D and 7E. Numbers were estimated from experimental data (see also Experimental Procedures). **(B)** Posterior range and median of each parameters calculated by Approximate Bayesian Computation (ABC) analysis from the experimental data to test the plausibility of the control parameters in **(A)**.